学位論文　（要約）

One-dimensional Azobenzene- and Bis(dipyrrinato)zinc(II)-linked Porphyrinic Wires – Synthesis and Photofunctionality

(アゾベンゼンおよびビス(ジピリナト)亜鉛(II)が架橋した一次元ポルフィリンワイヤー －合成と光機能)

平成 28 年度 7 月博士(理学)申請

東京大学大学院理学系研究科
化学専攻

MUSTAFAR SUZALIZA
ムスタファル　スザリザ

Abstract

This thesis describes a series of studies on the synthesis of one-dimensional porphyrinic wires and the exploration of their functionalities. Two kinds of starting materials were used for the construction of the porphyrinic wires. One is an aniline-porphyrin hybrid and the other one is a dipyrrin-porphyrin hybrid. These porphyrin monomers were chosen because of their interesting light absorption properties. Two methods were employed to fabricate those wires. In Chapter 1, the introduction to porphyrin, dipyrrin, and their properties as well as the application were discussed comprehensively. The application of porphyrin and its derivatives as explained briefly in this chapter.

In Chapter 2, the preparation and properties of azobenzene-linked porphyrinic wires were described. The wires were successfully fabricated by electrochemical polymerisation. The advantages of electrochemical polymerisation were mentioned in this chapter. Electrochemical polymerisation was proven to be an excellent method to immobilised the porphyrin monomer on various solid substrates. The film characterisation was done by various techniques in order to understand the physical and chemical properties of the film. The functionality of these wires also been studied. The wires were exhibited photocurrent generation ability upon light irradiation.

In Chapter 3, the fabrication of bis(dipyrrinato)zinc(II)-linked porphyrinic wires were discussed. The hybridization between dipyrrin and porphyrin was a good approach to improve the wire's photochemical properties. These wires were prepared by simple metal complexation between zinc ion and dipyrrin moiety. The photofunctionality of this showed some improvement upon this hybridization. These wires also exhibited a photocurrent generation ability upon light irradiation.

In Chapter 4, the summary of this series of research is described. In conclusion, both methods either electropolymerization or metal complexation can be engaged to fabricate one-dimensional wires. Since porphyrin can absorb light intensely, these wires shown good photofunctionality.

CONTENTS

CHAPTER 1

GENERAL INTRODUCTION

1.1 Porphyrins and its properties

A series of valuable characteristics, such as developed π-conjugation, intense color, rigid structure, and high chemical stability, allow porphyrins to be utilized in broad application areas like electronics,[1] medicine,[2] catalysis[3] and so forth. In particular, because of their versatility in light absorptions and redox activities, porphyrins are frequently used in optoelectronics[4] and photovoltaics[5] applications. With adequate electron transfer ability and capability to acquire light in wide wavelengths, porphyrins become eminent in light-induced electron donating systems, leading to applications in dye-sensitized solar cells[6,7,8] and bulk heterojunction solar cells.[9,10,11] The word porphyrin originated from porphura, purple in Greek language. All porphyrin and its derivatives do have colors. It is known that reduced form of porphyrins have dark or blue color whilst uncharged porphyrins red in color. The simplest porphyrin is porphine which made up from four pyrrolic compounds, connected by methyne bridges. Several examples of porphyrin derivatives are shown in Figure 1.1

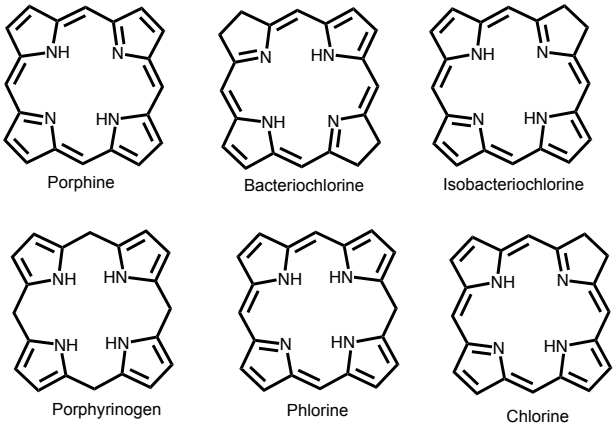

Figure 1.1: Example of several porphyrin derivatives. This figure is reproduced from ref. 12. Copyright 2002 Elsevier.

In general, porphyrins have planar structure with 22 π conjugated electrons. However, as shown in Figure 1.2,[13] only 18 π conjugated electrons are counted in one delocalized pathway abide by Hückel's 4n+2 rule. The two excluded double bonds from delocalization pathways are prone to be reduced or oxidized.[14,15]

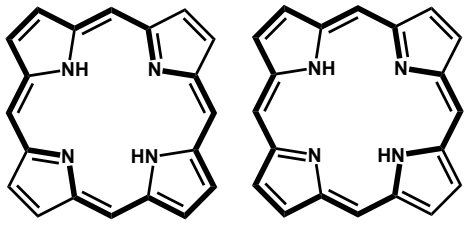

Figure 1.2. Delocalization pathways in porphyrin macrocycles. This figure is reproduced from ref. 13. Copyright 1988 Royal Science Society.

In porphyrin nomenclature, two systems were established known as Fischer and IUPAC nomenclature (Figure 1.3). In Fischer nomenclature, Greek alphabets are used to label carbon at meso positions. However, this nomenclature system suffered from lack of identification for all carbon on porphyrin skeleton. On the other hand, IUPAC nomenclature successfully overcomes the major drawback facing by Fischer nomenclature by named all carbon on porphyrin skeleton.

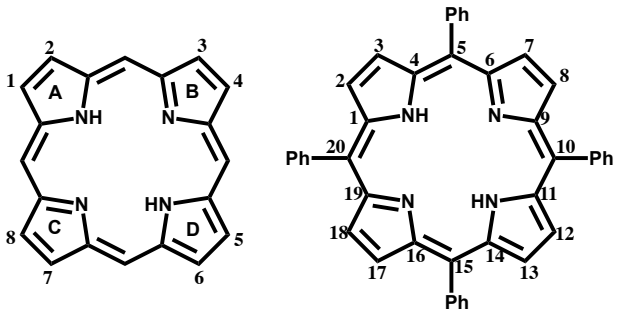

Figure 1.3: Comparison between Fischer (left) and IUPAC (right) nomenclature systems. This figure is reproduced from ref. 16. Copyright 1988 John Wiley & Sons, Inc.

Porphyrins and its derivatives can be synthetically synthesized as well as naturally found in nature.[17] For instance, heme[18] and chlorophyll[19] are two well-known naturally occurring porphyrin compounds. Heme is an iron-containing complex which act as oxygen carriers. On the other hand, chlorophylls are the magnesium-porphyrin compounds which converting light energy into chemical energy in photosynthesis system.

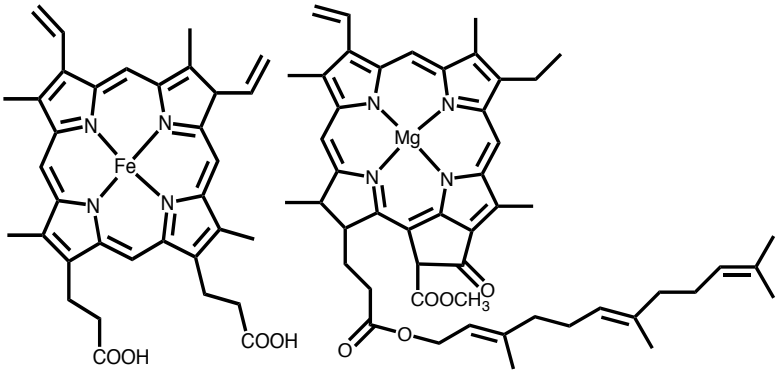

Figure 1.4 : Heme[18] and chlorophyll a. This figure is reproduced from ref. 18. Copyright 2014 American Chemical Society and from ref 19. Copyright 1990 Elsevier.

Owing to its robust structure, porphyrin macrocycles are known to have high thermal and chemical stabilities. Besides that, porphyrin and its derivatives also have intense electronic absorption and emission. As shown in Figure 1.5, an intense band within blue region commonly appears in UV-vis absorption spectra of porphyrins. This band is known as Soret band which represents the macrocyclic conjugation in porphyrin skeleton. The destruction of aromatic pathway can be easily identified by abnormality of Soret band. Eventually, the Soret band will remains unchanged if 18 π-electron cyclic pathway is preserved upon any reaction. Besides Soret band, another visible spectrum with adequate intensity can be noticed in the range of 500 to 600 nm. These bands are called Q bands and commonly appears four in free base porphyrin spectrum or two in metalloporphyrins.[20]

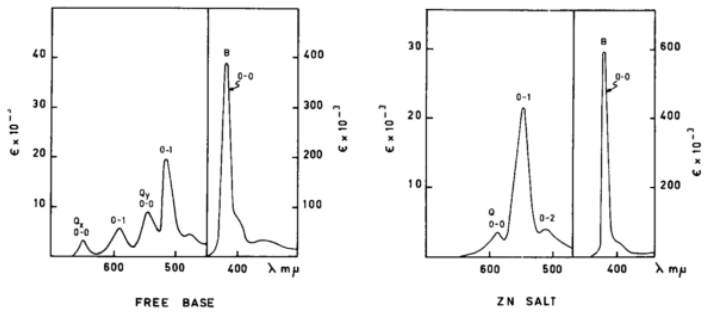

Figure 1.5: Absorption spectra of tetraphenylporphin. This figure is reprint from ref. 20. Copyright 1951 American Chemical Society.

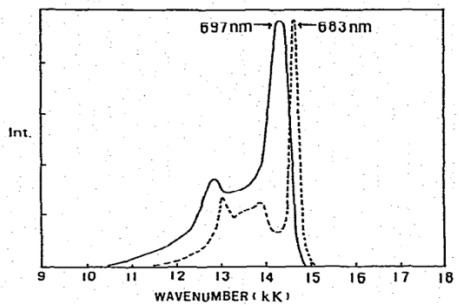

Figure 1.6: Luminescence spectra of CuMPDE 77 K. This figure is reprint from ref. 21. Copyright 1983 Elsevier.

The present of substituents and substituents arrangement directly influence the light absorbance as well as the appearance of porphyrins. Apart from just simply introduced substituents to porphyrin macrocycles, the properties of porphyrins can also be change by inserting suitable metal at the center of porphyrin core. Metalation directly influence electronic and binding properties which cause distinctive characteristics between metalloporphyrins and free base porphyrins. Generally, only free base porphyrins or closed shell metal complexes are known to exhibit fluorescence.[22] For instance, free base and zinc(II) porphyrins show both fluorescence and phosphorescence but copper(II) exhibit luminescence only at low temperatures (Figure 1.6).[23]

The NMR spectroscopy is one of the reliable technique to study porphyrin structures. The large aromatic ring current of the delocalization of π-electrons causes anisotropic effects in proton NMR.[24] This effect causes NMR signals for protons at meso position appear at low field, normally around δ 8 and 9 ppm whilst signals for shielded protons such as interior nitrogen-bound proton can be seen at very high field around δ -4 to -2 ppm. The carbon atoms in ^{13}C NMR of porphyrin are named by Greek alphabet which denoted as α pyrrolic, β pyrrolic and meso carbons. Peak of α carbons usually resonates around 145 ppm and 130 ppm for β carbon. In the case of meso carbon, the peaks usually spot around 120 ppm. Line broadening in α pyrrolic carbon signal is due to NH tautomerism. Nevertheless, this effect is easily suppressed by metalation or deprotonation.[25]

1.2 Synthesis of Porphyrins

1.2.1 Adler-Longo's method

The meso-substituted porphyrins could not naturally occur in nature[26] like β-substituted porphyrins. However, meso-substituted porphyrin is absolutely important in various application especially in material chemistry. Tetraphenylporphyrin (TPP) is the easiest meso-substituted porphyrin known to be synthesized. TPP can be simply prepared by reacting pyrrole with benzaldehyde in the present of a Lewis acid. Rothermond[27] was recognized as the pioneer in synthesizing meso-substituted porphyrin. He successfully conducted the reaction in sealed glass tubes at high temperature.[28] Even though this method can synthesized TPP, it faced major drawback by producing very low amount of TPP and producing tetraphenylchlorin as side reaction.

Noticing the problem facing by Rothermund's method, Adler and Longo[29] introduced new approach that afforded high yield up to 20-25% which is superior compared to Rothemond's method. Scheme 1 illustrates the general Adler-Longo synthesis. TPP can be synthesized by simple condensation of pyrrole in propionic acid at reflux in the present of oxygen which is necessary to oxidize the porphyrinogen intermediate. Despite producing better yield, this method also suffers from some limitation to synthesis symmetrical porphyrins. For instances, the harsh reaction condition such as refluxing at 141^0C cause aldehyde with sensitive groups such as hydroxyl, thiol and amino are not possible to be used in fabrication of meso-substituted porphyrins. This kind of limitation affect the functionality of TPP as building blocks in materials chemistry.[30] In addition, this method also has purification problem caused by high level of tar as well as poor reproducibility.

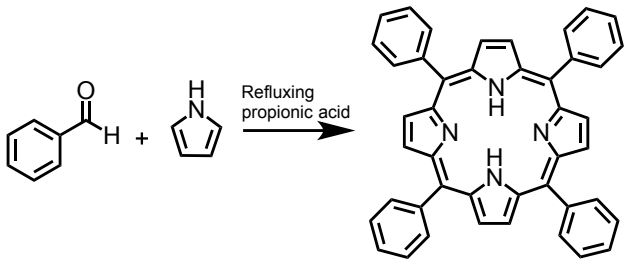

Scheme 1: General Adler-Longo synthetic scheme. This figure is reproduced from ref. 29. Copyright 1967 American Chemical Society.

1.2.2 Lindsey's method

In more recent years, Lindsey's group[31] proposed an excellent synthesis method which in ideal case, yields up to 50%. This method was developed from several hypotheses which were proven correct. They firstly proposed tetraphenylporphyrinogen was the product of condensation between benzaldehyde and pyrrole.[32] The high reactivity rate of benzaldehyde and pyrrole helps to predict the unnecessity of high temperature for reaction to take place. They tried to conduct the condensation reaction between benzaldehyde and pyrrole at room temperature and succeed getting porphyrin as reaction product. Whereas later, condensation at room temperature became major merit for this method which make the synthesis condition milder. The reaction between pyrrole and aldehyde can proceed by adding catalytic amount of Lewis acid such as $BF_3.OEt_2$ or trifluoroacetic acid (TFA) in chlorinated solvents (Scheme 2). The gentleness in this method allows different substituted porphyrins (like A_2B_2 or A_3B) to be prepared from one pot reaction. This contributes to the numerous different meso-substituted porphyrins which can be synthesized and utilized as important building blocks for further synthesis.[33] Presence of oxidant such as tetrachloro-1,4-benzoquinone (p-chloranil) or 2,3-dichloro-5,6-dicyano-1,4-benzoquinone (DDQ) is important to oxidize the unstable porphyrinogen to form the porphyrin macrocycles. Although this method is really promising in meso-substituted porphyrin synthesis, some aldehydes which bearing large ortho-substituents or very electron-poor group cannot be engaged in synthesis. Tedious work out also needed in purification process, but worthy if separation can be achieved because different substituted porphyrins could be prepared by one pot reaction which is favorable in organic synthesis.

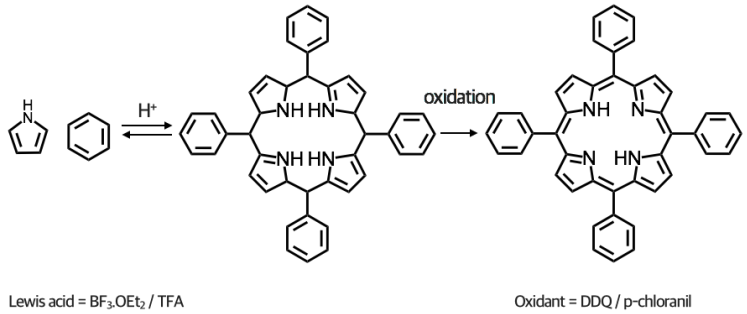

Scheme 2: General Lindsey's synthethic scheme. This figure is reproduced from ref. 31. Copyright 1987 American Chemical Society.

1.2.3 Condensation of dipyrromethanes

Fischer[34] introduced self-condensation of dipyrromethene at high temperature up to 200°C in the presence of organic acid such as tartaric or succinic acid. Scheme 3 showed general synthetic scheme proposed by Fischer. Two different dipyrromethenes bearing non-sensitive substituents such as alkyl group are employed in the fabrication of porphyrin macrocycles. The condensation condition at high temperature became a limitation in introducing sensitive substituents on dipyrromethene ring.

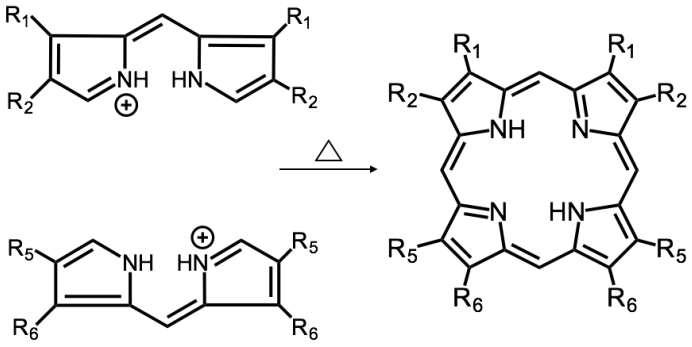

Scheme 3: General synthetic scheme proposed by Fischer. This figure is reproduced from ref. 35. Copyright 2016 Royal Society of Chemistry.

Subsequently, MacDonald[36] improves Fischer's method and known as "2+2" MacDonald's condensation. This method employs dipyrromethanes instead of dipyrromethenes (Scheme 4). The milder condensation condition makes this synthetic reaction more promising in terms of fabricating porphyrin with various substituents. Unfortunately, this synthetic method also has some weakness. For example, dipyrromethanes prone to decomposed in acidic reagents which contributes to scrambling or redistribution to occur.

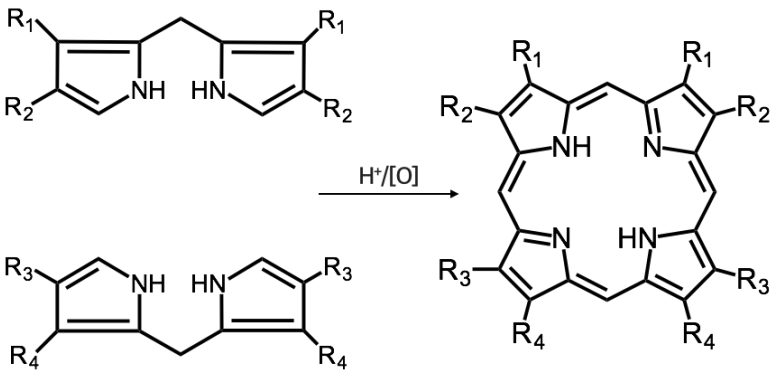

Scheme 4: General synthetic scheme proposed by MacDonald. This figure is reproduced from ref. 35. Copyright 2016 Royal Society of Chemistry.

1.3 Dipyrrin-porphyrin Hybridized

In Chapter 3, synthesis of bis(dipyrrinato)zinc(II) linked porphyrinic wires will be discussed comprehensively. Therefore, it is worth to give general introduction of dipyyrin in this chapter. In fact, conjugated systems between porphyrin and dipyrrin have attracted the attention of many researchers due to their remarkable optical and electronic properties.[37] Carbon atoms in dipyrrin structure are numbered as shown in Figure 1.7. Substituent groups generally integrated at meso position. Dipyrrin and its derivatives are widely used as monoanionic bidentate ligand that has ability to form numerous complexes either with main or transition elements[38]. For instance, different coordination geometry and complexation stoichiometry will be achieved when dipyrrin forms complexes with metal ions such Zn, Cu, In, Ga, Sn and so forth. These differences give diversity in properties and applications.[39,40,41] However, dipyrrin-boron (BODIPYs) complexes relatively more prominent compare to other complexes because of their strong and tunable fluorescence properties. The interesting optical properties exhibited by hybrization of porphyrin-dipyrrin derivatives as in Figure 1.8 has intrigue interest of many researchers to engage it as a functional π-conjugated system in numerous purposes[42] such as fabrication light harvesting arrays for molecular based solar cells,[43] optoelectronic gates[44] and so forth. Moreover, Lindsey *et al*. also reported dipyrrin metal complexes as bridging units for energy transfer systems consisting of porphyrins.[45]

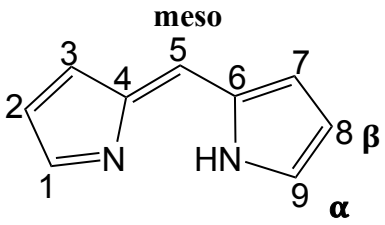

Figure 1.7: Carbon numbering in dipyrrin structure.

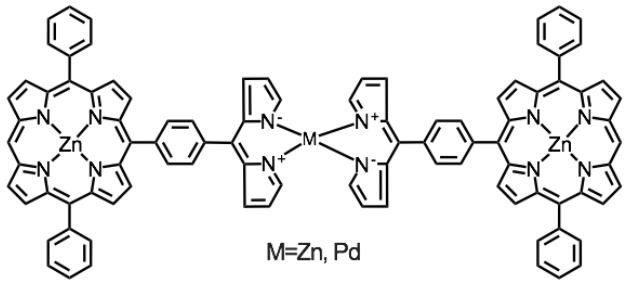

Figure 1.9: An example of dipyrrin metal complexes as bridging units. This figure is reproduced from ref.45. Copyright 2003 American Chemical Society.

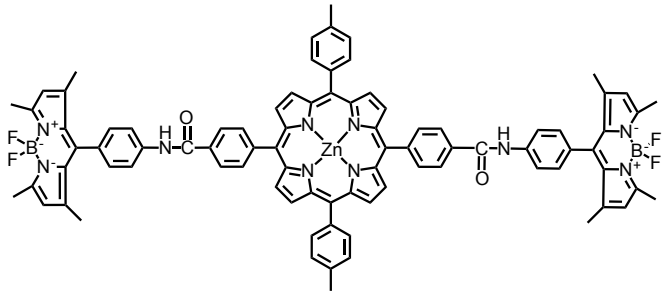

Figure 1.8: An example of hybridization between dipyrrin derivative and porphyrin. This figure is reproduced from ref. 47. Copyright 2010 Royal Society of Chemistry.

1.4 Application of Porphyrins

1.4.1 Electronics

Planarity and strong π-conjugation in its structure cause porphyrin as a favourable candidate to be employed in fabrication of various electronic devices. π-conjugated molecules are known to exhibit successful charge transport property ascribed to effective overlapping of π-orbitals.[48] Therefore, porphyrin derivatives are preferable in constructing electron delocalizing systems.[49] For instance, an appropriate synthetic array could emerge as molecular photonic wires (Figure 1.10). Molecular photonic wires and molecular electronic wires are totally distinguishable. Molecular photonic wires transfer excited state energy while molecular electronic wires support electron or hole transfer.[50] The general design of photonic wires are generally resembles the synthetic light-harvesting system which consist of input and output unit. Other than that, metalloporphyrins have also been extensively studied to be used in fabrication of molecular electronics (Figure 1.13),[51] as sensitizer in solar cells (Figure 1.11),[52,53] memory devices (Figure 1.12)[54] and so forth.

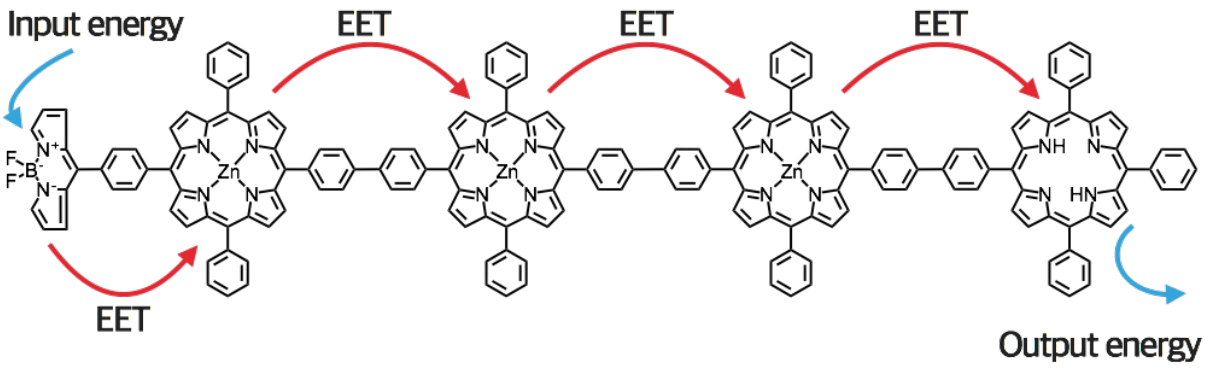

Figure 1.10: Illustration of a photonic molecular wires. Input unit is Bodipy-based dye, zinc porphyrin as bridging unit and free-base porphyrin as emitting output unit. This figure is reproduced from ref. 55. Copyright 2015 Royal Society of Chemistry.

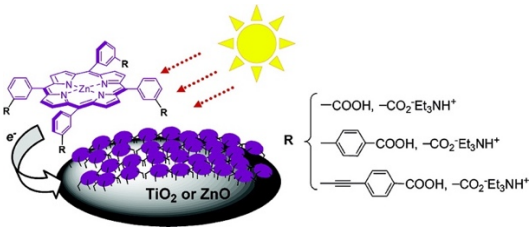

Figure 1.11: Porphyrin as sensitizer in fabrication of solar cell. This figure is reprint from ref. 53. Copyright 2007 American Chemical Society.

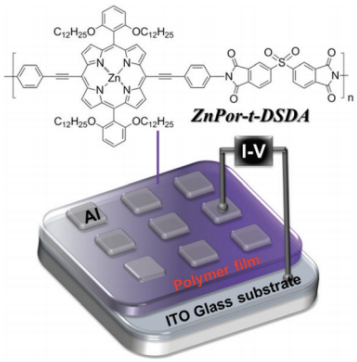

Figure 1.12: The diagram illustrates the application of porphyrin film in resistive memory device. This figure is reprint from ref. 54. Copyright 2016 American Chemical Society.

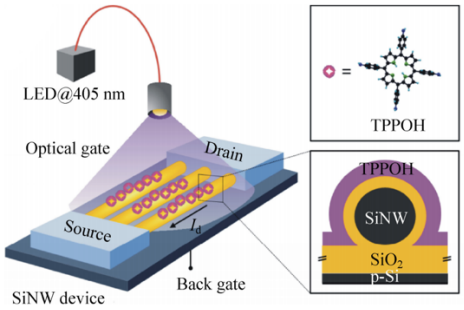

Figure 1.13: An illustration of hybrid light sensitive silicon nanowires-based filed effect transistor. This figure is reprint from ref. 56. Copyright 2015 Springer.

1.4.2 Medicine

Figure 1.14 summarize several porphyrin-based biomaterial and its applications in medical field. For example, fluorescence imaging is a useful tool for medical imaging[57] owing to it relatively inexpensive and brief exposure time. π - π stacking between the porphyrin molecules will cause porphyrin molecules start to aggregate. These aggregations known as J- or H- aggregation will affect the absorption bands and subsequently shifted the absorption peaks towards longer wavelength.[57] This properties make porphyrins useful as inexpensive fluorescence dye with emission wavelength in the NIR region.[58] Porphyrins and its derivatives also known to form metalloporphyrin complexes chelated with diverge range of metal ions which make them potentially high to be engage in radiotheraphy and multimodal imaging modalities.[59] Apart from that, porphyrins also widely used in magnetic resonance imaging (MRI) because of noninvasively and high spatial resolution.[60] Photodynamic therapy (PDT)[61] by engaging porphyrin as the photosensitizer in cancer therapy has been widely practiced. This kind of therapy helps to minimize destruction effect to healthy tissues close to the tumor cells. In PDT, a photosensitizer will absorb light at certain wavelength and get excited to a singlet state and subsequently to a triplet state. The excess energy then transfers to molecular oxygen and then the molecular oxygen get excites to a highly reactive singlet state. In this state, singlet oxygen is cytotoxic and has the ability to destroy tumor cells.[62]

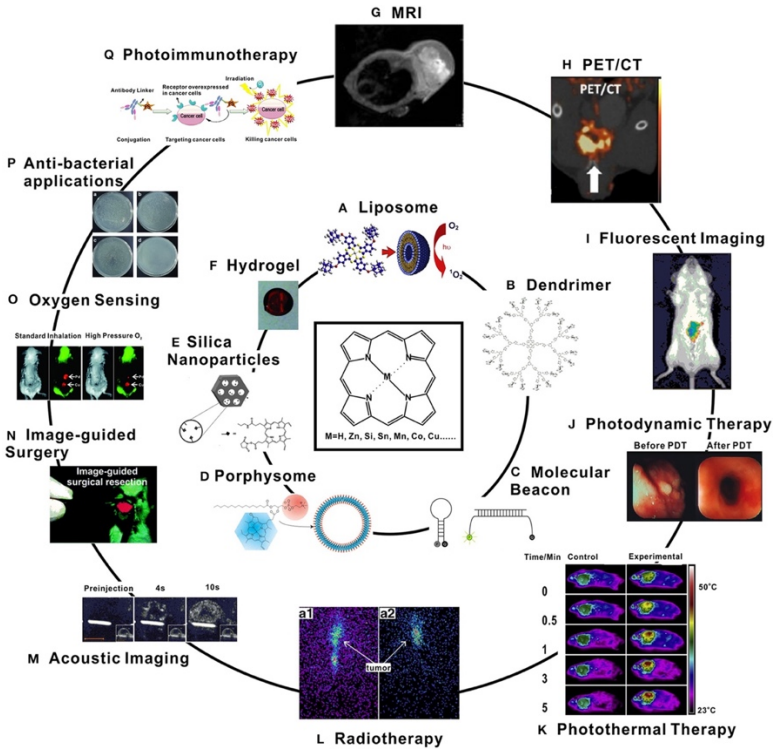

Figure 1.14. Several examples of porphyrin-based biomaterials (inner circle) and their applications (outer circle). This figure is reprint from ref. 63. Copyright 2015 Springer.

1.5 Coordination polymers

Coordination polymers (CP) are metal-ligand compounds that can be either in one (1D), two (2D) or three dimensions (3D) depending on the geometries of bridging organic linkers and coordination modes of metal ions (Figure 1.15).[64] 3D CPs which also known as metal-organic framework (MOF) are highly ordered array of three dimensional coordination compounds. This 3D CPs have been studied for many years due to their excellent functionalities that can be engaged in catalysis,[65] sorbent for toxic industrial chemicals,[66] drug delivery[67] and light harvesting.[68] Eventually, 2D CPs exhibit unique properties. For instance a 2D nickel bis(dithiolene) complex nanosheet acts as an electronic conductor[69] because of large overlap between metal d orbitals and ligand π orbital. Owing to increasing studies done in exploring functionalities of 2D CPs, many proton-conducting CPs[70] as well as other properties such as 2D luminescence CP[71] also been reported. On the other hand, one dimensional coordination polymer is the simplest array in its class. CPs generally fabricated by self-assembly. For instance, metalloporphyrin polymers can easily prepared by mixing various bridging ligands[72,73,74,75] and metal ions in suitable organic solvent. Such polymers were successfully synthesized by coordination between nitrogenous ligands and metal ions such as ruthenium, osmium or iron.[76]

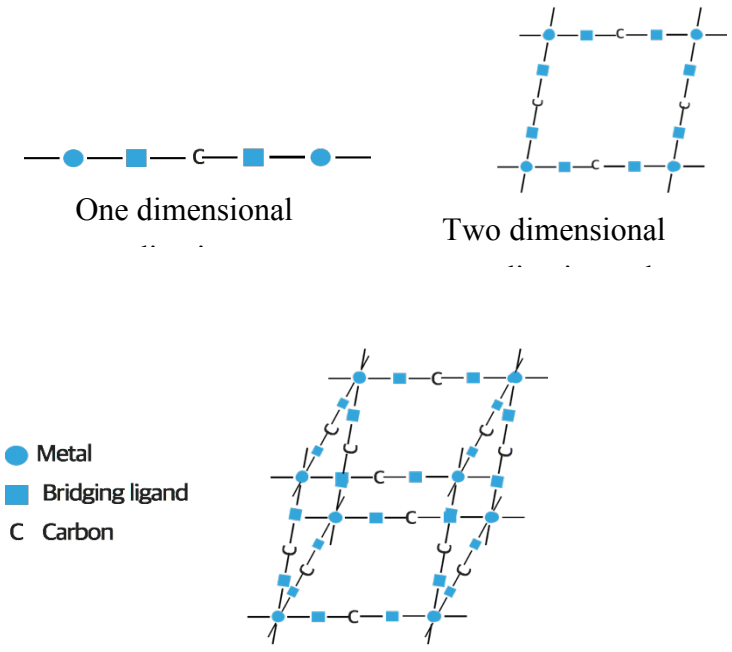

Figure 1.15: Examples of coordination polymers. This figure is reproduced from ref. 77. Copyright 2003 Royal Society of Chemistry.

1.6 Covalent polymer

Covalent polymers principally obtained by relatively simple chemical[78] or electrochemical method. For instance, several reports have discovered the achievability of direct polymerization of porphyrins via a meso–meso coupling.[79] Osuka *et al*. have succeeded in preparing extremely long meso-meso-coupled porphyrin arrays based on the chemical oxidation of zinc diarylporphyrins by employing $Ag^{I}PF_6$ (Figure 1.16) as oxidant.[80] Aside from that, since the discovery done by Macor and Spiro,[81] the formation of covalent polymers more relies on the use of oxidative[82] or reductive[83] radical coupling of porphyrins via substituents on the ring periphery.[84]

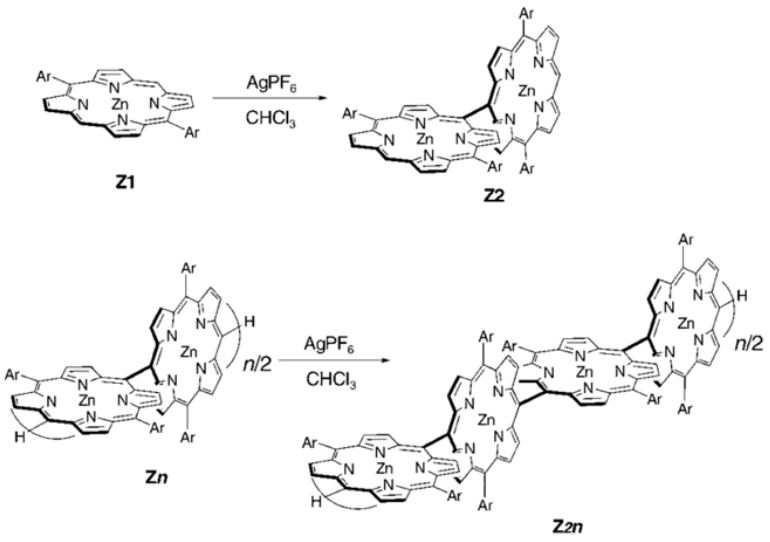

Figure 1.16: Examples of long porphyrin arrays prepared by chemical oxidation. This figure is reprint from ref. 80. Copyright 2000 John Wiley & Sons, Inc.

1.7 Immobilization of Porphyrins on Various Solid Supports

1.7.1 Electrochemical polymerization

For decades, various methods[85,86,87] for porphyrins immobilization on different solid support have been numerously reported. One of renowned immobilization process is electrochemical polymerization which offers distinctive advantages such as strong film attachment to the surface, ability to control film thickness, tolerancy toward other chemical functions on the aryl moiety and so on. Although the electropolymerization appears to be a simple process to immobilized porphyrinic films on solid support, this method typically needs an essential step which consists synthesis of the starting monomeric porpyrin subunit composed of electropolymerizable substituents such as vinyl, amino,[88] hydroxylphenyl, pyrrolyl,[89] carbazolyl,[90,91] thienyl,[92] or pyridyl[93] groups. The appropriate scanning to certain potential will generate corresponding radicals, which initiate further polymerization between monomers.[94] On the other hand, a direct coupling[95] as well as nucleophilic attacks[96] onto porphyrin cation radicals have been reported as other alternative in the porphyrin polymerization. This nucleophilic attack was applied to the electrosynthesis of a porphyrinate-viologen wire and cationic porphyrin copolymers bearing an appropriate Lewis base as substituent.[97] In the case of aryl radical grafting, Stevenson *et al.* proposed that the generated polymeric film may strongly be physisorbed to ITO surface[98] although the detailed information is unclear. In this research, aniline-substituted porphyrins at meso position were electropolymerized and azobenzene-linkages were generated in the polymeric film structure. Glassy carbon (GC), ITO and tin oxide (SnO_2) were employed as solid surfaces towards the exploration of photofunctionality exhibited by the films.

1.7.2 Molecular self-assembly

Bottom-up or self-assembly approach is known to give structural control as well as versatility in nanofabrication. The idea of self-assembly was taken from the work of Langmuir and Blodgett[99] in 1935. In 1946, Bigelow *et al.*[100] found out long chain alkylamines can form a densely packed monolayer on platinum surface. However, the term self-assembly was not really used to describe the formation of well-ordered molecular monolayer at that moment. The term self-assembly started to be mentioned when Nuzzo and Allara discovered the formation of close-packed monolayers of chemisorbed alkyl thiolate molecules when contacted with gold surfaces.[101] The formation of molecular crystals,[102] colloids,[103] lipid bilayers/monolayer,[104] and self-assembled monolayer[105] are all examples of molecular self-assembly. Nowadays, molecular self-assembly is widely adapted in numerous applications including electronics,[106] energy storage and conversion,[107] biomedical[108] and so forth. Molecular self-assembly can be defined as a process in which molecules or part of molecules spontaneously form ordered aggregates.[109] Figure 1.17 shows general steps in preparing SAMs on solid substrate. When a suitable substrate is immersed in a ligand solution, attraction and repulsion between molecules leads to self-assembling. The essential component in fabricating SAMs on solid substrate are tether, linker and a suitable substrate. During the formation of SAMs, tether compounds will form certain bonding with solid substrate and form ordered structure. In general, several interactions like van der Waals and electrostatic interactions, hydrophobic interactions, hydrogen bonds and so forth will form in self-assembly. Thus, weak covalent bond and coordination bond have also been reported.[110] In the case of gold substrate, when the clean gold substrate is immersed into thiol solution,[111] self-assembly rapidly takes place and produces highly ordered films by forming coordination bond between thiol and gold atoms. Not only limited to thiol, other moieties like disulfide,[112] thiocyanate[113] are also commonly used to fabricate SAMs on gold substrate because gold is known to have excellent thermal and electric conductivity, inert against heat, humidity, oxidation and numerous chemical reactions. Other solid substrates such as ITO and silicon are generally used for self-assembly. For example, the transparency of ITO makes it possible to be employed as electrodes in dye-sensitized solar cells as well as in organic electric luminescence devices

because the compatibility of ITO for photoirradiation. Several chemical compounds such as phosphoric acid, trialkoxysilane,[114] thiophene or carboxylic acid[115] are generally used for ITO surface modification.[116]

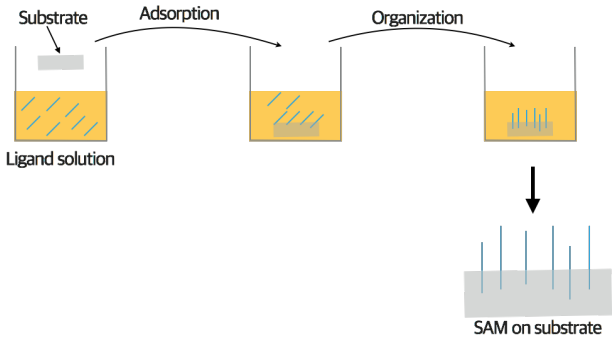

Figure 1.17: General steps in preparing SAMs on solid substrate. This figure is reproduced from ref. 116. Copyright 2005 American Chemical Society.

1.7.3 Stepwise-surface modification

Surface modifications by SAMs are primarily based on monolayer systems with simple chemical structures. Integration of multifunctional molecules in self-assembly will cause the synthesis becomes more complicated and unfavorable. Therefore, layer-by-layer assembled by stepwise surface modification is being developed to grant easy fabrication of more complex molecular structure by facile approach. Since this method offers the flexibility in tailoring metal ions and functional ligands, this method appears to be really promising in material science because the diversity and functionality of ligands are really important in fabricating many molecular building blocks. In stepwise surface modification, a template is firstly prepared by self-assembly.[117,118] Meanwhile, electropolymerization on a SAM-modified surface were also reported and successfully fabricated a multilayer structure.[119] Besides that, stepwise coordination reactions are also useful to synthesize oligomeric molecular wires with the desired number of complex units and hetero-layered structures. This method basically involves sequential immersion into solutions of metal ions and bridging ligands as shown in Figure 1.18. A suitable substrate which acts as the template needs to be immersed in certain amount of time in an anchor ligand solution. After that, the modified substrate is dipped into a metal source solution containing a metal ion which commonly inorganic metal salts.[120] Next, the metal-ion-terminated substrate is immersed into bridging ligand solution, which has a number of coordination sites. Thus, a one-layer metal complex wire is prepared. By controlling the repetitive number of substrate being immersed into metal ion and bridging ligand solution, the length of polymers can easily be monitored. A handful reports on fabrication of multilayer using stepwise coordination were for linear wires[121] with various metal complex oligomer and polymer wires. However, the emerging research of branched structures using ligand with more coordination sites continue flourishing (Figure 1.19).[122]

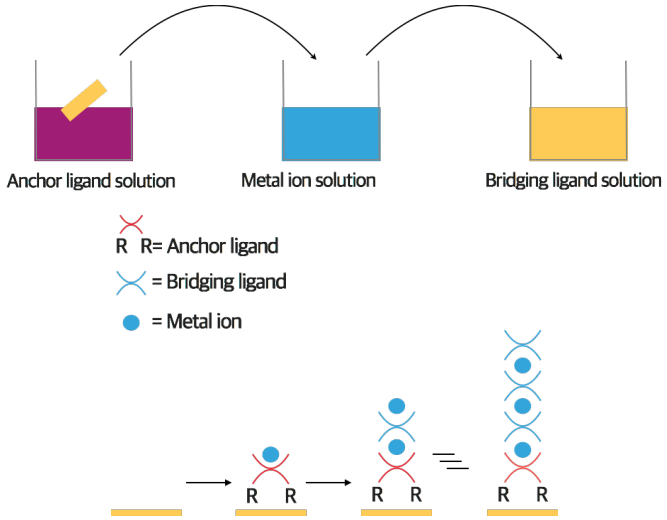

Figure 1.18: Illustration of stepwise coordination reaction in constructing the multilayer structure. This figure is reproduced from ref. 120. Copyright 2004 American Chemical Society.

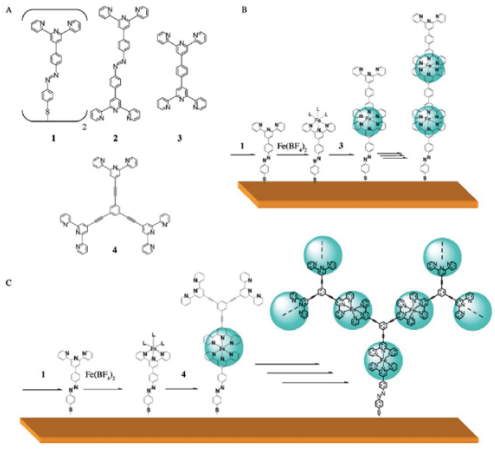

Figure 1.19: Schematic of ligand (A), linear (B) and branched (C) oligomer wires prepared by stepwise coordination reaction. This figure is reprint from ref. 122. Copyright 2007 John Wiley & Sons, Inc.

1.8 Aim of This Thesis

In my PhD study, two different porphyrins wires were developed using two different polymerization methods. As mentioned before, various polymerization techniques have been developed to immobilize monomers on solid substrates. Out of these numerous techniques, I used electrochemical polymerization to fabricate the first porphyrinics wires because of simplicity and functionality offered by this technique. In this study, I engaged simple porphyrin structure to be immobilised on solid substrate in order to explore the formation azo-linkage during electropolymerization. Since the polymerized film exhibited photofunctionality, this study will open the possibilities to integrate other substituents into the porphyrin design. In fabricating second porpyrinic wires, simple metal complexation reaction was engaged. The wires were fabricated in order to explore the photofunctionality of hybridized dipyrrin-porphyrin monomer.

1.9 References

1. Park, W. J., Chae, S. H., Shin, J., Choi, D. H. and Lee, S. J. Semiconducting π-extended porphyrin dimer and its characteristics in OFET and OPVC. *Synth. Met.* **205,** 206–211 (2015).
2. Deng, X., Liang, Y., Peng, X., Su, T., Luo, S., Cao, J., Gu, Z. and He, B. A facile strategy to generate polymeric nanoparticles for synergistic chemo-photodynamic therapy. *Chem. Commun.* **2000,** 2–5 (2015).
3. Tseberlidis, G., Zardi, P., Caselli, A., Cancogni, D., Fusari, M., Lay, L. and Gallo, E. Glycoporphyrin catalysts for efficient C–H bond aminations by organic azides. *Organometallics* **34**, 3774-3781 (2015).
4. Li, Y., Wang, W., Leow, W.R., Zhu, B., Meng, F., Zheng, L. and Chen, X. Optoelectronics of organic nanofibers formed by co-assembly of porphyrin and perylenediimide. *Small* **10,** 2776–81, 2740 (2014).
5. Xie, Y., Tang, Y., Wu, W., Wang, Y., Liu, J., Li, X., Tian, H. and Zhu, W. H. Porphyrin cosensitization for a photovoltaic efficiency of 11.5%: A record for non-ruthenium solar cells based on iodine electrolyte. *J. Am. Chem. Soc.* **137,** 14055–14058 (2015).
6. Gasiorowski, J., Pootrakulchote, N., Reanprayoon, C., Jaisabuy, K., Vanalabhpatana, P., Sariciftci, N.S. and Thamyongkit, P. Porphyrin containing lipophilic amide groups as photosensitizer for dye-sensitized solar cells. *RSC Adv.* **5,** 72900–72906 (2015).
7. Mai, C.-L., Moehl, T., Hsieh, C-H., Decoppet, J-D., Zakeeruddin, S.M., Gratzel, M. and Yeh, C-Y. Porphyrin sensitizers bearing a pyridine-type anchoring group for dye-sensitized solar cells. *ACS Appl. Mater. Interfaces* **7,** 14975–14982 (2015).
8. Chen, J., Sheng, Y., Ko, S., Liu, L., Han, H. and Li, X. Push–pull porphyrins with different anchoring group orientations for fully printable monolithic dye-sensitized solar cells with mesoscopic carbon counter electrodes. *New J. Chem.* **39,** 5231–5239 (2015).
9. Kumar, C.V., Cabau, L., Koukaras, E.N., Sharma, A., Sharma, G.D. and Palomarea, E. A-π-D-π-A based Porphyrin for solution processed small molecule bulk hetero junction solar cells. *J. Mater. Chem. A* **3,** 16287–16301 (2015).

10. Gao, K. Li, L., Lai, T., Xiao, L., Huang, Y., Huang, F., Peng, J., Cao, Y., Liu, F., Russel, T.P, Janssen, R. A. J. and Peng, X. Deep absorbing porphyrin small molecule for high performance organic solar cells with very low energy losses. *J. Am. Chem. Soc.* **137**, 7282-7285 (2015).
11. Kesters, J., Verstappen, P., Kelchtermans, M., Lutsen, L., Vanderzande, D. and Maea, W. Porphyrin-based bulk heterojunction organic photovoltaics: The rise of the colors of life. *Adv. Energy Mater.* **5**, 1500218 (2015).
12. Kadish, K. M., Smith, K. M., Guilard, R. The porphyrin handbook: Inorganic, organometallic and coordination chemistry, *Volume 3*. Elsevier (2000).
13. Abraham, R. J., Medforth, C. J., Mansfield, K. E., Simpson, D. J. and Smith, K. M. Nuclear magnetic resonance spectra of porphyrins. part 33.' ring currents in Nickel(II) hydroporphyrins derived from anhydromesorhodoporphyrin XV. *J. Chem. Soc. Pekin Trans. II* 1365-1372 (1988).
14. Bergonia, H. A., Phillips, J. D. and Kushner, J. P. Reduction of porphyrins to porphyrinogens with palladium on carbon. *Anal. Biochem*. **384**, 74-78 (2009).
15. Whitlock, Jr., H.W., Hanauer,R., Oester, M. Y. and Bower, B.K. Diimide reduction of porphyrins. *J. Am. Chem. Soc.* **91,** 7485–7489 (1969).
16. Moss, G. P. & College, Q. M. Nomenclature of tetrapyrroles. *Eur. J. Biochem.* **328,** 277–328 (1988).
17. Wyllie, G. R. A., Silvernail, N. J., Oliver, A. G., Schulz, C. E. & Scheidt, W. R. Iron nitrosyl "natural" porphyrinates: Does the porphyrin matter? *Inorg. Chem.* **53,** 3763–8 (2014).
18. Poulos, T. L. Heme enzyme structure and function. *Chem. Rev*. **114**, 39119-3962 (2014).
19. Woodward, R.B., Ayer, W.A., Beaton, J. M., Bickelhaupt, F., Bonnet, R., Buchschacher, P., Closs, G.L, Dutler, H., Hannah, J., Hauck, F.P., Ito, S., Langemann, A., Goff., E.L., Leimgruber, W., Lwowski, W., Sauer, J., Valenta, Z. and Volz, H. The total synthesis of chlorophyll a. *Tetrahedron* **46,** 7599–7659 (1990).
20. Dorough, G. D., Miller, J. R. and Huennekens, F. M. Spectra of the Metallo-derivatives of α,β,γ,δ-Tetraphenylporphine. *J. Am. Chem. Soc.* **73,** 4315–4320

(1951).

21. Konishi, S., Hoshino, M. and Imamura, M. Luminescence of the copper porphyrin aggregate. *Chem. Phys. Lett.* **94,** 267–269 (1983).
22. Becker, R.S. and Allison, J.B. Metalloporphyrins. Electronic spectra and nature of perturbations. 11. Group IIa, IIb, and IVa derivatives 1a. J. Phy. Chem. **67**, 2669-2675 (1963).
23. Harriman, A. Luminescence of porphyrins and metalloporphyrins Part 1. Zinc(II), nickel(II) and manganese(II) porphyrins. **76,** J.C.S. Faraday 1, 1978-1985 (1980).
24. Mamaev, V. M., Ponamarev, G. V, Zenin, S. V & Evstigneeva, R. P. Ring currents and nuclear magnetic resonance in porphyrins. *Teor. i Eksp. Khimiya* **6,** 40–46 (1970).
25. Abraham, R. J., Hawkes, G. E., Hudson, M. F. and Smith, K. M. The nuclear magnetic resonance spectra of porphyrins. Part X. Carbon-13 nuclear magnetic resonance spectra of some meso-tetraarylporphyrins and their metal chelates. *J. Chem. Soc. Perkin Trans. 2* **204** (1975).
26. Lindsey, J. S. Synthetic Routes to meso-patterned porphyrins. *Acc. Chem. Res.* **43**, 300-311 (2010).
27. Paul, R. Formation of porphyrins from pyrrole and aldehydes. *J. Am. Chem. Soc.* **57,** 11–12 (1935).
28. Rothemund, P. A New porphyrin synthesis. The synthesis of porphin. *J. Am. Chem. Soc.* **58,** 625–627 (1936).
29. Adler, A.D., Longo, F.R., Finarelli, J.D., Goldmacher, J., Jacques, A. and Leonard, K. A simplified synthesis for meso-tetraphenylporphin. *J. Org. Chem.* **32,** 476 (1967).
30. Vicente, M. da G. H. and Smith, K. M. Syntheses and functionalizations of porphyrin macrocycles. *Curr. Org. Synth.* **11,** 3–28 (2014).
31. Lindsey, J. S., Schreiman, I. C., Hsu, H. C., Kearney, P.C. and Marguerettaz, A.M. Rothemund and Adler-Longo reactions revisited: Synthesis of tetraphenylporphyrins under equilibrium conditions. *J. Org. Chem.* **52,** 827–836 (1987).
32. Merhi, A. Synthesis of new organic and organometallic porphyrin assemblies for

optics. (2014).

33. Aratani, N., Takagi, A., Yanagawa, Y., Matsumoto, T., Kawai, T., Yoon, Z.S., Kim, D. and Osuka, A. Giant meso-meso-linked porphyrin arrays of micrometer molecular length and their fabrication. *Chem. Eur. J.* **11,** 3389–3404 (2005).
34. Fischer, H. and Zeile, K. Synthese des Hämatoporphyrins, Protoporphyrins und Hämins. *Justus Liebig's Ann. der Chemie* **468,** 98–116 (1929).
35. Smith, K. M. Development of porphyrin syntheses. *New J. Chem.* doi:10.1039/c6nj00820h
36. Arsenault, G. P.,Bullock, E. and MacDonald S.F. Pyrromethanes and porphyrins therefrom. *J. Am. Chem. Soc.* **82,** 4384–4389 (1960).
37. Ozdemir, M., Choi, D., Kwon, G., Zorlu, Y., Cosut, B., Kim, H., Facchetti, A., Kim, C. and Usta, H. Solution-processable BODIPY-based small molecules for semiconducting microfibers in organic thin-film transistors. *ACS Appl. Mater. Interfaces* **8**, 14077-14087 (2016).
38. Nabeshima, T., Yamamura, M., Richards, G. J., and Nakamura, T. Design and synthesis of dipyrrin complexes bearing unique structures, properties and functions. *J. Synth. Org. Chem., Jpn.* **73,** 57–65 (2015).
39. Sakamoto, N., Ikeda, C., Yamamura, M. and Nabeshima, T. Structural interconversion and regulation of optical properties of stable hypercoordinate dipyrrin silicon complexes. *J. Am. Chem. Soc.* **133,** 4726–4729 (2011).
40. Maeda, H. and Ito, M. Dipyrrin–porphyrin hybrids: Potential π-conjugated platform to fabricate coordination oligomers. *Chem. Lett.* **34,** 1150–1151 (2005).
41. Sakamoto, R., Hoshiko, K., Liu, Q., Yagi, T., Nagayama, T., Kusaka, S., Tsuchiya, M., Kitagawa, Y., Wong, W-Y. and Nishihara, H. A photofunctional bottom-up bis(dipyrrinato)zinc(II) complex nanosheet. *Nat. Commun.* **6,** 6713 (2015).
42. Imamura, T. and Fukushima, K. Self-assembly of metallopyridylporphyrin oligomers. *Coord. Chem. Rev.* **198,** 133–156 (2000).
43. Topka, M. R. and Dinolfo, P. H. Synthesis, characterization, and fluorescence properties of mixed molecular multilayer films of BODIPY and Zn(II) tetraphenylporphyrins. *ACS Appl. Mater. Interfaces* **7,** 8053–8060 (2015).
44. Ambroise, A., Wagner, R. W., Rao, P. D., Riggs, J. A., Hascoat, P., Diers, J. R.,

Seth, J., Lammi, R. K., Bocian, D. F., Holten, D. and Lindsey, J. S. Design and synthesis of porphyrin-based optoelectronic gates. *Chem. Mater.* **13,** 1023–1034 (2001).

45. Yu, L., Muthukumaran, K., Sazanovich, I.V., Kirmaler, C., Hindin, E., Diers, J.R., Boyle, P. D., Bocian, D. F., Holten, D. and Lindsey, J. S. Excited-state energy-transfer dynamics in self-assembled triads composed of two porphyrins and an intervening bis(dipyrrinato)metal complex. *Inorg. Chem.* **42,** 6629–6647 (2003).
46. Wagner, R. W. and Lindsey, J. S. Boron-dipyrromethene dyes for incorporation in synthetic multi-pigment light-harvesting arrays. *Pure Appl. Chem* **68,** 1373–1380 (1996).
47. Maligaspe. E, Kumpulainen. T, Subbaiyan, N.K, Zandler, M.E, Lemmetyinen. H, Tkachenko. N.V and D'Souza, F. Electronic energy harvesting multi BODIPY-zinc porphyrin dyads accommodating fullerene as photosynthetic composite of antenna-reaction center. *Phys. Chem. Chem. Phys.* **12,** 7434–7444 (2010).
48. Cornil, J., Brédas, J.-L., Zaumseil, J. and Sirringhaus, H. Ambipolar transport in organic conjugated materials. *Adv. Mater.* **19,** 1791–1799 (2007).
49. Vasilopoulou, M., Douvas, A. M., Georgiadou, D. G., Constantoudis, V., Davazoglou, D., Kennou, S., Palilis, L. C., Daphnomili, D., Coutsolelos, A. G. and Argitis, P. Large work function shift of organic semiconductors inducing enhanced interfacial electron transfer in organic optoelectronics enabled by porphyrin aggregated nanostructures. *Nano Res.* **7,** 679–693 (2014).
50. Wagner, R. W. and Lindsey, J. S. A molecular photonic wire. *J. Am. Chem. Soc.* **116,** 9759–9760 (1994).
51. Liljeroth, P. Molecular electronics: Flipping a single proton switch. *Nat. Nanotechnol.* **7,** 5–6 (2011).
52. Wang, H., Xiao, L., Yan, L., Chen, S., Zhu, X., Peng, X., Wang, X., Wong, W-K. and Wong, W-Y. Structural engineering of porphyrin-based small molecules as donors for efficient organic solar cells. *Chem. Sci*. **7**, 4301-4307 (2016).
53. Rochford, J., Chu, D., Hagfeldt, A. and Galoppini, E. Tetrachelate porphyrin chromophores for metal oxide semiconductor sensitization: Effect of the spacer length and anchoring group position. *J. Am. Chem. Soc.* 129, 4655-4665.

54. Tsai, M.-C., Wang, C-L., Lin, C-Y., Tsai, C-L., Yen, H-J., You, H-C and Liou, G-S. A novel porphyrin-containing polyimide for memory devices. *Polym. Chem.* **7,** 2780–2784 (2016).

55. Harriman, A. Artificial light-harvesting arrays for solar energy conversion. *Chem. Commun.* **51,** 11745–11756 (2015).

56. Baek, E., Pregl, S., Shaygan, M., Romhildt, L., Weber, M. W., Mikolajick, T., Ryndyk, D. A., Baraban, L. and Cuniberti, G. Optoelectronic switching of nanowire-based hybrid organic/oxide/semiconductor field-effect transistors. *Nano Res.* **8,** 1229–1240 (2015).

57. Würthner, F., Kaiser, T. E. and Saha-Möller, C. R. J-aggregates: From serendipitous discovery to supramolecular engineering of functional dye materials. *Angew. Chem. Int. Ed. Engl.* **50,** 3376–410 (2011).

58. Hayashi, K., Nakamura, M. and Ishimura, K. Silica–porphyrin hybrid nanotubes for in vivo cell tracking by near-infrared fluorescence imaging. *Chem. Commun.* **48,** 3830-3832 (2012).

59. Zhang, Y. and Lovell, J. F. Porphyrins as theranostic agents from prehistoric to modern times. *Theranostics* **2,** 905- 915 (2012).

60. Jing, L., Liang, X., Li, X., Lin, L., Yang, Y., Yue, X. and Dai, Z. Mn-porphyrin conjugated Au nanoshells encapsulating doxorubicin for potential magnetic resonance imaging and light triggered synergistic therapy of cancer. *Theranostics* **4,** 858–871 (2014).

61. Varamo, M., Loock, B., Maillard, P. and Grierson, D. S. Development of strategies for the regiocontrolled synthesis of meso-5,10,20-triaryl-2,3-chlorins. *Org. Lett.* **23,** 4689–4692 (2007).

62. Wróbel, D. and Dudkowiak, A. Porphyrins and phthalocyanines – Functional molecular materials for optoelectronics and medicine. *Mol. Cryst. Liq. Cryst.* **448,** 15/[617]–38/[640] (2006).

63. Huang, H., Song, W., Rieffel, J. and Lovell, J. F. Emerging applications of porphyrins in photomedicine. *Front. Phys.* **3**:23 (2015).

64. Zhu, Q.-L. and Xu, Q. Metal–organic framework composites. *Chem. Soc. Rev.* **43,** 5403–6176 (2014).

65. Mccarthy, B. D., Martin, D. J., Rountree, E. S., Ullman, A. C. and Dempsey, J. L. Electrochemical reduction of Brønsted acids by glassy carbon in acetonitrile−Implications for electrocatalytic hydrogen evolution. *Chem. Commun*. **53**, 8350-8361 (2014).

66. Wilcox, O. T., Fateeva, A., Katsoulidis, A. P., Smith, M. W., Stone, C. A. and Rosseinsky, M. J. Acid loaded porphyrin-based metal–organic framework for ammonia uptake. *Chem. Commun* **51,** 14989–14991 (2015).

67. Lin, W., Hu, Q., Jiang, K., Yang, Y., Yang, Y., Cui, Y. and Qian, G. A porphyrin-based metal–organic framework as a pH-responsive drug carrier. *J. Solid State Chem.* **237,** 307–312 (2016).

68. So, M. C., Wiederrecht, G. P., Mondloch, J. E., Hupp, J. T. and Farha, O. K. Metal–organic framework materials for light-harvesting and energy transfer. *Chem. Commun.* **51,** 3501–3510 (2015).

69. Kambe, T., Sakamoto, R., Hoshiko, K., Takada, K., Miyachi, M., Ryu, J-H., Sasaki, S., Kimi, J., Nakazato, K., Takata, M. and Nishihara, H. π-conjugated nickel bis(dithiolene) complex nanosheet. *J. Am. Chem. Soc*. **137**, 2462-2465 (2013).

70. Sengupta, A., Datta, S., Su, C., Herng, T. S., Ding, J., Vittal, J. J. and Loh, K. P. Tunable electrical conductivity and magnetic property of the two dimensional metal organic framework $[Cu(TPyP)Cu_2(O_2CCH_3)_4]$. *ACS Appl. Mater. Interfaces*. **8**, 16154-16159 (2016).

71. Huh, S., Jung, S., Kim, Y., Kim, S.-J. and Park, S. Two-dimensional metal–organic frameworks with blue luminescence. Dalton Trans. **39**, 1261-1265 (2009).

72. Zha, Q., Ding, C., Rui, X and Xie, Y. A novel porphyrin-based ligand containing four 4,4'- dipyridylamine moieties: Syntheses, structures, and luminescent properties of Mn(II), Cu(II), Zn(II), and Cd(II) coordination polymers. *Cryst. Growth Des.* **13**, 4583–4590 (2013).

73. Ikbal, S. A., Brahma, S. and Rath, S. P. Building-up remarkably stable magnesium porphyrin polymers self-assembled via bidentate axial ligands: Synthesis, structure, surface morphology, and effect of bridging ligands. *Inorg. Chem.* **51,** 9666–9676 (2012).

74. Ren, G.-J., Liu, Y.-Q. and Liu, S.-J. Two novel metal-organic frameworks based

on linear dicarboxylic acid and 5-(4-pyridyl)tetrazole. *J. Solid State Chem.* **232,** 79–82 (2015).

75. Dong, D., Yu, N., Cong, Y., Zhao, Y., Zhao, H., Liu, D., Li, Z., Liu, J. and Liu, D. In-situ hydrothermal preparation of a novel 3D CuI-based tetrazole coordination polymer with pseudo-porphyrin secondary building units. *Inorg. Chem. Commun.* **62,** 1–4 (2015).
76. Collman, J. P., McDevitt, J.T., Leidner, C.R., Yee, G.T., Torrance, J.B. and Little, W. A. Synthetic, electrochemical, optical, and conductivity studies of coordination polymers of iron, ruthenium, and osmium octaethylporphyrin. *J. Am. Chem. Soc.* **109,** 4606–4614 (1987).
77. Janiak, C. Engineering coordination polymers towards applications. *Dalt. Trans.* 2781–2804 (2003).
78. Ozawa, H., Kawao, M., Tanaka, H. and Ogawa, T. Synthesis of dendron-protected porphyrin wires and preparation of a one-dimensional assembly of gold nanoparticles chemically linked to the π-conjugated wires. *Langmuir* **23**(11), 6365–6371 (2007).
79. Osuka, A and and Shimidzu, H. Meso-meso-linked porphyrin arrays. *Angew. Chem. Int. Ed.* **36**, 135–137 (1997).
80. Aratani, N., Osuka, A., Kim, Y. H., Jeong, D. H. Extremely long, discrete meso-coupled porphyrin arrays. *Angew. Chem. Int. Ed.* 39, **8**, 1458–1462 (2000).
81. Macor, K. and Spiro, T. G. Porphyrin electrode films prepared by electrooxidation of metalloprotoporphyrins. *J. Am. Chem. Soc.* 5601–5607 (1983).
82. Zhang, H., Zhang, Y., Gu, C. and Ma, Y. Electropolymerized conjugated microporous poly(zinc-porphyrin) films as potential electrode materials in supercapacitors. *Adv. Energy Mater.* **5,** 1402175 (2015).
83. Huang, S. and Lin, C. Reductive electropolymerization of N-methyl-3-pyridylethynylporphyrins. *Chem, Commun*. **51**, 519-521(2014).
84. Yuasa, M., Oyaizu, K., Yamaguchi, A., Ishikawa, M., Eguchi, K., Kobayashi, T., Toyoda, Y. and Tsutsuki, S. Structure and redox properties of electropolymerized film obtained from iron meso-tetrakis(3-thienyl)porphyrin. *Polym.Adv.Technol.* **16**, 616–621 (2005).

85. Grabowska, I., Zborowska, M., Nguyen, N. T., Dehaen, W., Stulz, E., Wood, J. W., Radecka, H. and Radecki, J. Deposition of Ni(II) porphyrin monolayer on the gold electrode via azide-alkyne click-coupling and its electrochemical characterization. *Int. J. Electrochem. Sci.* **9,** 5948–5960 (2014).

86. Matsumoto, R., Yonemura, H. and Yamada, S. Photoelectrochemical responses from zinc porphyrin-silver nanoparticle composite films fabricated on ito electrodes. *J. Phys. Chem. C* **117,** 2486–2493 (2013).

87. Maurin, A. and Robert, M. Noncovalent immobilization of a molecular iron-based electrocatalyst on carbon electrodes for selective, efficient CO_2-to-CO conversion in water. *J. Am. Chem. Soc.* **138,** 2492–5 (2016).

88. Mustafar, S., Wu, K-H., Toyoda, R., Takada, K., Maeda, H., Miyachi, M., Sakamoto, R. and Nishihara, H. Electrochemical fabrication of one-dimensional porphyrinic wires on electrodes. *Inorg. Chem. Front.* **3**, 370-375 (2016).

89. Bedioui, F., Devynck, J. and Claude, B-C. Immobilization of metalloporphyrins in electropolymerized films: Design and applications. *Acc. Chem. Res.* **28,** 30–36 (1995).

90. Durantini, J., Otero, L., Funes, M., Durantini, E. N., Fungo, F. and Gervaldo, M. Electrochemical oxidation-induced polymerization of 5,10,15,20-tetrakis[3- (N-ethylcarbazoyl)]porphyrin. Formation and characterization of a novel electroactive porphyrin thin film. *Electrochim. Acta* **56,** 4126–4134 (2011).

91. Zhang, H., Zhang, Y., Gu, C. and Ma, Y. Electropolymerized conjugated microporous poly(zinc-porphyrin) films as potential electrode materials in supercapacitors. *Adv. Energy Mater.* **5,** 1–6 (2015).

92. Takechi, K., Takahashi, N., Shiga, T., Akiyama, T. and Yamada, S. An influence of monomeric porphyrin structure on the electropolymerized photoactive electrode for polymer solar cells. *Mol. Cryst. Liq. Cryst.* **538,** 10–14 (2011).

93. Xia, Y., Schaming, D., Farha, R. and Ruhlmann, L. Bis-porphyrin copolymers covalently linked by pyridinium spacers obtained by electropolymerization from β-octaethylporphyrins and pyridyl-substituted porphyrins. *New J.* **36**, 588–596 (2012).

94. Giraudeau, A., Schaming, D., Hao, J., Farha, R., Goldmann, M. and Ruhlmann, L.

A simple way for the electropolymerization of porphyrins. *J. Electroanal. Chem.* **638,** 70–75 (2010).

95. Ogawa, T., Nishimoto, Y., Yoshida, N., Ono, N. and Osuka, A. Completely regioselective synthesis of directly linked meso,meso and meso,β porphyrin dimers by one-pot electrochemical oxidation of metalloporphyrins. *Angew. Chem., Int. Ed.* **38,** 176–179 (1999).
96. Varamo, M., Loock, B., Maillard, P. and Grierson, D. S. Development of strategies for the regiocontrolled synthesis of meso-5,10,20-triaryl-2,3-chlorins. *Org. Lett.* **9,** 4689–4692 (2007).
97. Hao, J., Giraudeau, A., Ping, Z. and Ruhlmann, L. Supramolecular assemblies obtained by large counteranion incorporation in a well-oriented polycationic copolymer. *Langmuir* **24,** 1600–1603 (2008).
98. Maldonado, S., Smith, T. J., Williams, R. D., Morin, S., Berton, E. and Stevenson, K. J. Surface modification of indium tin oxide via electrochemical reduction of aryldiazonium cations. *Langmuir* **22,** 2884–2891 (2006).
99. Langmuir, V. I. and Blodgettl, K. B. Ober einige neue methoden zur untersuchung yon monomolekularen filmen. Kollo I D-Zeitsch Ri Ft, 257-263 (1935).
100. Bigelow, W. C., Pickett, D. L. and Zisman, W. A. Oleophobic monolayers: I. Films adsorbed from solution in non-polar liquids. *J. Colloid. Sci.* 1(6), 513-538 (1946).
101. Nuzzo, R. G. and Allara, D. L. Adsorption of bifunctional organic disulfides on gold surfaces. *J. Am. Chem. Soc.* **105,** 4481–4483 (1983).
102. Pathak, S. K., Pradhan, B., Gupta, R. K., Gupta, M., Kumar, S. P. and Achalkumar, A. S. Aromatic π-π Driven supergelation, aggregation induced blue light emission, tunability of the self-assembly and emission in star-shaped 1,2,4-oxadiazole derivatives. *J. Mater. Chem. C* (2016). doi:10.1039/C6TC01939K
103. Qiao, F., Xu, W., Liu, M., Yang, J., Cui, X., Wang, Q., Bian, J. and Kim, D. H. Effect of Cd-phosphonate complex on the self-assembly structure of colloidal nanorods. (2016). doi:10.1016/j.matlet.2016.05.106
104. Shimizu, T., Kameta, N., Ding, W. and Masuda, M. Supramolecular self-assembly into bio-functional soft nanotubes: From bilayers to monolayers. *Langmuir* (2016). doi:10.1021/acs.langmuir.6b01632

105. Galanti, A., Kototva, O., Blasco, S., Johnson, C. J., Peacock, R. D., Mills, S., Boland, J. J. Albrecht, M. and Gunnlaugsson, T. Exploring the effect of ligand structural isomerism in Langmuir-Blodgett films of chiral luminescent Eu ^{III} self-assemblies. *Chem. - A Eur. J.* (2016). doi:10.1002/chem.201600560

106. Jin, J., Lee, D., Im, H.-G., Han, Y. C., Jeong, E. G., Rolandi, M., Choi, K. C. and Bae, B. -S. S. Chitin nanofiber transparent paper for flexible green electronics. *Adv. Mater.* (2016). doi:10.1002/adma.201600336

107. Samant, S. P., Grabowski, C. A., Kisslinger, K., Yager, K. G., Yuan, G., Satija, S. K., Durstock, M. F., Raghavan, D and Karim, A. Directed self-assembly of block copolymers for high breakdown strength polymer film capacitors. *ACS Appl. Mater. Interfaces* **8,** 7966–7976 (2016).

108. Zhang, J., Liu, K., Müllen, K. and Yin, M. Self-assemblies of amphiphilic homopolymers: Synthesis, morphology studies and biomedical applications. *Chem. Commun.* **51,** 11541–11555 (2015).

109. Whitesides, G. M. and Boncheva, M. Beyond molecules: Self-assembly of mesoscopic and macroscopic components. PNAS **99**(8), 4769-4774 (2002).

110. Stang, P. J., Olenyuk, B., Whiteford, J. A. and Fechtenkötter, A. Self-assembly of nanoscale cuboctahedra by coordination chemistry. *Nature* **398,** 796–799 (1999).

111. Häkkinen, H. The gold–sulfur interface at the nanoscale. *Nat. Chem.* **4** (2012).

112. Acero Sánchez, J. L., Fragogo, A., Joda, H., Suarez, G., Mc Neil, C. J., O'Sullivan, C. K. Site-directed introduction of disulfide groups on antibodies for highly sensitive immunosensors. *Anal. Bioanal. Chem.* **408**(19), 5337-5346 (2016).

113. Ciszek, J. W., Keane, Z. K., Cheng, L., Stewart, M. P., Yu, L. H., Natelson, D. and Tour, J. M. Neutral complexes of first row transition metals bearing unbound thiocyanates and their assembly on metallic surfaces. *J. Am. Chem. Soc.* **128,** 3179–3189 (2006).

114. Muthurasu, A. and Ganesh, V. Electrochemical characterization of self-assembled monolayers (SAMs) of silanes on indium tin oxide (ITO) electrodes--tuning electron transfer behaviour across electrode-electrolyte interface. *J. Colloid Interface Sci.* **374,** 241–249 (2012).

115. Yan, C., Zharnikov, M., Gölzhä, A. and Grunze, M. Preparation and

characterization of self-assembled monolayers on indium tin oxide. *Langmuir* **16**, 6208-6215 (2000).

116. Love, J. C., Estroff, L. A., Kriebel, J. K., Nuzzo, R. G. and Whitesides, G. M. Self-assembled monolayers of thiolates on metals as a form of nanotechnology. Chem. Rev. 105 (4), 1103-1169 (2005).
117. Ciampi, S., Bocking, T., Kilian, K. A., James, M., Harper, J. B. and Gooding, J. J. Functionalization of acetylene-terminated monolayers on Si(100) surfaces: A click chemistry approach. Langmuir **23**, 9320-9329 (2007).
118. Maeda, H., Sakamoto, R. & Nishihara, H. Metal complex oligomer and polymer wires on electrodes: Tactical constructions and versatile functionalities. *Polym.* **54,** 4383–4403 (2013).
119. Bolat, G., Kuralay, F., Eroglu, G. and Abaci, S. Fabrication of a polyaniline ultramicroelectrode via a self assembled monolayer modified gold electrode. *Sensors.* **13,** 8079–94 (2013).
120. Doron-Mor, I., Cohen, H., Cohen, S. R., Popovitz-Biro, R., Shanzer, A., Vaskevich, A. and Rubinstein, I. Layer-by-layer assembly of ordinary and composite coordination multilayers. Langmuir **20**, 107727-10733 (2004).
121. Sakamoto, R., Katagiri, S., Maeda, H. & Nishihara, H. Bis(terpyridine) metal complex wires: Excellent long-range electron transfer ability and controllable intrawire redox conduction on silicon electrode. *Coord. Chem. Rev.* **257,** 1493–1506 (2013).
122. Nishimori, Y., Kanaizuka, K., Murata, M. and Nishihara, H. Synthesis of molecular wires of linear and branched Bis(terpyridine)- complex oligomers and electrochemical observation of through-bond redox conduction. *Chem. - An Asian J.* **2,** 367–376 (2007).

CHAPTER 2

AZOBENZENE-LINKED PORPHYRIN WIRES FORMED BY ELECTROCHEMICAL POLYMERIZATION

2.1 Introduction

In particular, porphyrin derivatives are known to exhibit versatility in light absorptions and redox activities. Therefore, porphyrins are frequently used in optoelectronics[1] and photovoltaics[2] applications. With adequate electron transfer ability and capability to acquire light in wide wavelengths, porphyrins become eminent in light-induced electron donating systems, leading to applications in dye-sensitized solar cells and bulk heterojunction solar cells.

Synthesizing porphyrinic polymers on solid surface is an important technique for applications.[3] Such polymer structures may be accomplished by various methods as discussed in Chapter 1. The preparation of thin porphyrin films on solid substrates demands for adequate methods to secure that the distinct physical and chemical properties of the molecule are integrated to the material. Through electropolymerization, the polymerization can be achieved either by electrooxidative or electroreductive[4] reaction. Among other techniques, porphyrin electropolymers were mostly generated by oxidizing instead of reducing the monomeric porphyrins in solution. Thus, the electrochemical oxidation of porphyrin monomers has been proven to be an excellent method in generating polymeric films covalently grafted to the electrode surface.[5] Strong film attachment to the surface become one advantage as well as the capability to control the layer thickness,[6] and its tolerance toward other chemical functions on the porphyrin moiety make electropolymerization a favorable technique.

In this research, the formation of azobenzene linkage upon electrooxidation is crucial to ensure the polymerization can be achieved. Azo linkage is known to exhibit multi functionalities as well as great properties such as can act as an electron conducting bridge,[7] has high thermal stability,[8] responsive to light irradiation and so forth. For instance, photo responsive properties of azo linkage lead to fabrication of liquid crystal.[9] Besides that, polymer containing azo linkage also exhibit another fascinating properties such as photoconductivity[10] and photochromism.[11,12] These multi functionalities contribute to the potential applications in sensors, photo switching as well as other photonic devices.

2.1.1 Aim of This Study

As mentioned in introduction, azo group is an interesting motif to be integrated into a polymer structure due to their stability and conductivity. By employing porphyrin monomer comprising anilino group, the tendency to covalently linked two porphyrin monomer is high. Therefore, in this study I fabricated azobenzene-linked porphyrin polymer (Figure 2.1) by engaging electrochemical oxidation to induce oxidative coupling. Since the modified electrode by thin films have many potential applications, three different electrodes have been used as solid substrates to immobilize the porphyrin monomer on it. Even though these three solid structures different from one another, the successful polymer immobilization on these electrodes will open the possibilities to engage these modified electrons in various application areas such as catalysis and light harvesting system. The generated polymeric film is expected to show photofunctionality, so that I engaged the modified ITO with this polymeric films in photocurrent generation measurement. Hence, the photofunctionality of the electropolymerized porphyrin film was disclosed along with the plausible mechanism for photoelectric conversion.

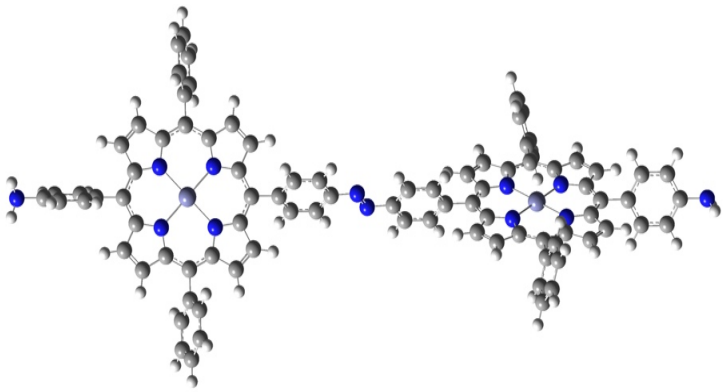

Figure 2.1: The porphyrinic wires comprising anilino substituents and azobenzene-linker.

2.2 Experimental Section

2.2.1 Reagents

All chemicals were purchased from Kanto Chemical Co., Tokyo Chemical Industry Co., Ltd, or Wako Pure Chemical Industries, Ltd, and used as received unless otherwise stated. **1** was synthesized according to previous literature studies with a few modifications.

2.2.2 Materials

The working electrode were made from a glassy carbon (GC) rod (Tokai Carbon Co. Ltd.), indium-tin oxide (ITO) on glass (5 Ω sq^{-1}) and tin oxide (SO_2). The glassy carbon rod was cut to 3 mm long pieces, washed with water and acetone and dried in 130^{o}C oven. The GC rod was then sealed in a Pyrex glass tube by gas-oxygen flame. The sealed GC electrode was polished by waterproof abrasive papers and finished by 0.3 μm Al_2O_3. ITO and SnO_2 was treated before use upon sonication in acetone (10 minutes) and non-ionic detergent in water (30 minutes × 2) and, and purified water (10 minutes). The cleaned substrates were stored in water, and dried by nitrogen blow just prior to use. The counter electrode was prepared by sealing platinum wire in a soda-lime glass, annealed with oxygen flame, and cooled down prior to use. In photofunctionality experiment, tetra-N-butylammonium perchlorate, Bu_4NClO_4, employed as a supporting electrolyte was purified by recrystallization from ethanol, and dried in vacuo. A Milli-Q purification system (Merck KGaA) was used to obtain pure water.

2.2.3 Instrumentations

All ^{1}H NMR data were recorded on a Bruker-DRX500 using $CDCl_3$ as the solvent and tetramethylsilane (δ_H = 0.00) as an internal standard. High-resolution fast atom bombardment mass spectrometry (HR-FAB-MS) was conducted using a JEOL JMS-700 MStation mass spectrometer. UV/vis spectra were obtained with a JASCO V-570 spectrometer. Raman spectra were recorded using a JASCO NRS-5100. AFM measurements were carried out using an Agilent Technologies 5500 scanning probe microscope in the high-amplitude mode (tapping mode) with a silicon cantilever Nano World PPP-NCL probe. FE-SEM images were recorded using JEOL JSM-7400FNT with an acceleration voltage of 1.5 kV. All experiments were carried out under an ambient condition unless otherwise stated. The molecular size of **1** was determined by DFT calculation. The DFT calculation was carried out using a Gaussian09 Revision D.01 program package. The geometry optimization was performed using B3LYP functional with the LANL2DZ basis set for Zn and 6-31g(d) basis set for the other atoms and the result was visualized using GaussView 5.0.8 software. Whilst for photofunctionality, a xenon lamp (MAX-302, Asahi Spectra Co., Ltd) was used as photon flux source and a monochromator (CT-10, JASCO Corporation) to monochromate the photon flux. An electrochemical analyser (ALS 750A, BAS Inc.) was used to control the electrode potential and photocurrent acquisition of the photoelectric conversion system. A photon counter (8230E and 82311B, ADC Corporation) was engaged in quantifying the photon flux of the incident light.

2.2.4 Photoelectric conversion ability measurements

The setup of photocurrent generation measurement is shown in Figure 2.2. The modified ITO electrode with **P1** (formed by 50 scan cycles) was assigned as a working electrode (photoanode). The UV-vis absorption of the modified ITO was measured at different position to assure the uniform film coverage on the modified electrode. The uniformity of film coverage on modified electrode is essential element to gain good result from photoelectric conversion measurement. An Ag/Ag^+ electrode (0.01 M $AgClO_4$ in 0.1 M Bu_4NClO_4/acetonitrile) acting as a reference electrode and a Pt wire as a counter electrode. All three electrodes were engaged in an acetonitrile solution of 0.1M Bu_4NClO_4 containing triethanolamine (TEOA, 0.05 M) as a sacrificial donor reagent. The cell was sealed and deoxygenized by argon bubbling for 5 minutes. An electrochemical analyzer was used to control the electrode potential and photocurrent acquisition of the photoelectric conversion system. Monochromatic light for an action spectrum (400–500 nm in every 10 nm) was extracted from a xenon lamp and a monochromator was utilized to monochromate the photon flux while a photon counter was engaged in quantifying the photon flux of the incident light for the quantum yield calculation. For the wavelength-dependent quantum yield measurement, the potential bias was fixed at -0.22 V *vs.* Ag^+/Ag. The size of the electrode active area was approximated from a fluorocarbon rubber o-shaped ring; 0.264 cm^2.

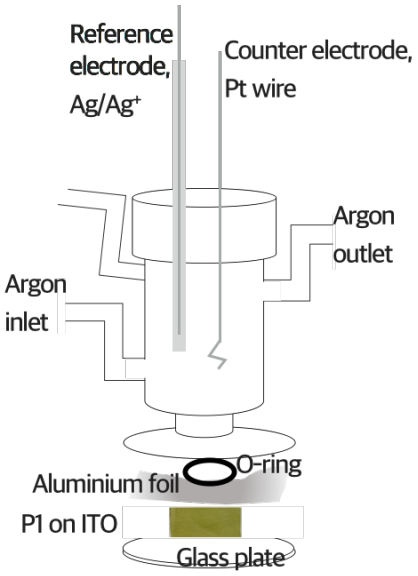

Figure 2.2: The schematic image of the electrochemical cell for the photoelectric conversion measurements.

2.2.5 Quantum efficiency (IQE)[13]

The quantum yield of photocurrent conversion, Φ was calculated by referring to Equation (1).

$$\Phi = n_e/n_p \quad (1)$$

n_e = number of mole of electrons that flow in the circuit per unit time (in mol s^{-1})

n_p = number of mole of photons absorbed by the sensitizer per unit time (in mol s^{-1})

thus, n_e were calculated using equations (2),

$$n_e = i/F, \quad (2)$$

while n_p was calculated using equation (3).

$$n_p = W\lambda[1\text{-}10^{-A}]/N_A hc, \quad (3)$$

I = current flow (in A)

F = Faraday constant (9.65×10^4 C mol^{-1})

W = photon flux of incident light (in J s^{-1})

λ = wavelength of the irradiated light (from 4.00×10^{-7} m to 5.00×10^{-7} m)

A = absorbance at the irradiated wavelength

N_A = Avogadro constant (6.02×1023 mol^{-1})

h= Planck constant (6.63×10^{-34} J s)

c= velocity of light (3.00×10^8 m s^{-1})

Hence, i was calculated using equation (4):

$$i = i_L - i_D, \quad (4)$$

i_L= average light current for the first cycle (10 s)

i_D = average dark current just before the illumination of light.

2.2.6 Synthesis of monomer (1)

Synthesis of 5-(4-nitrophenyl)dipyrromethane (S1)[14]

Pyrrole (44 mL, 630 mmol) and 4-nitrobenzaldehyde (3.83 g, 25.4 mmol) were added to a 200 mL of triple-neck round-bottomed flask and degassed with a stream of N_2 for 15 min. Then, trifluoroacetic acid (0.20 mL, 2.60 mmol) was added to the mixture. The solution was stirred under N_2 at room temperature for 10 min and then quenched with 0.1 M NaOH aq. The organic phase was extracted with dichloromethane and washed with water. The organic layer then dried over Mg_2SO_4, and the solvent was removed after filtration under reduced pressure. Purification was performed by column chromatography on silica gel using CH_2Cl_2: hexane (3:1) as eluent. Yellow solid was obtained as the final product (5.035 g, 74.4% yield). Mp: 157.5−159.2 ^oC; ^1H NMR (500 MHz, $CDCl_3$) δ 8.20 (d, J = 8.82 Hz, 2H), 8.02 (br s, 2H), 7.39 (d, J = 8.35 Hz, 2H), 6.77-6.78 (m, 2H), 6.21 (q, J = 3.03 Hz, 2H), 5.89 (s, 2H), 5.61 (s, 1H).

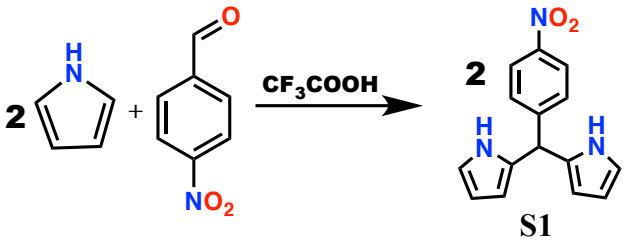

S1

Synthesis of 5,15-di(4-nitrophenyl)-10,20-diphenylporphyrin (S2)[15]

Compound **S1** (1.0 g, 3.7 mmol) and benzaldehyde (0.40 g, 3.7 mmol) were dissolved in 500 mL of anhydrous dichloromethane under N_2. The reaction mixture and trifluoroacetic acid (15.2 mL, 194 mmol) were cooled at 0 ^{0}C with an ice bath and a PTFE cannula was used to add the acid slowly into the reaction mixture. The reaction vessel was protected from light by wrapping with aluminum foil and the reaction mixture was stirred at 0 ^{0}C for 40 minutes. Chloranil (1.84g, 7.48 mmol) was then added and the mixture continuously stirred at room temperature for 1 hour. Then, the reaction was quenched by adding triethylamine (27 mL, 190 mmol). Organic phase was washed with water and dried over $MgSO_4$. The solvent was evaporated under reduced pressure and column chromatography was conducted on silica gel with dichloromethane as eluent. Purple solid was obtained as the final product (1.513 g, 57.45% yield). Mp >320 ^{o}C; ^{1}H NMR (500 MHz, $CDCl_3$) δ 8.91 (d, J = 4.61 Hz, 4H), 8.76 (d, J = 4.71 Hz, 4H), 8.65 (d, J = 8.46 Hz, 4H), 8.41 (d, J = 8.39 Hz, 4H), 8.21 (d, J = 7.42 Hz, 4H), 7.75-7.82 (m, 6H), -2.78 (s, 2H).

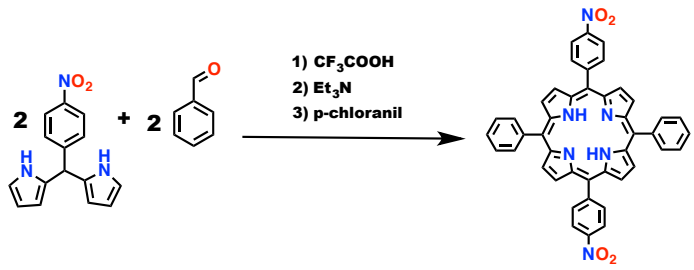

S1 **S2**

Synthesis of 5,15-di(4-aminophenyl)-10,20-diphenylporphyrin (S3)[16]

Compound **S2** (0.5 g, 0.71 mmol) was dissolved in 300 mL of concentrated hydrochloric acid under N_2. $SnCl_2.2H_2O$ (0.96 g, 4.26 mmol) was added to the solution, and refluxed for 4 hours. The reaction mixture left to cool, and cold water was added to quench the reaction. Then, pH of the reaction mixture was adjusted to pH 8-9 with concentrated ammonium hydroxide. Dichloromethane was added to extract the organic phase and dried over $MgSO_4$. The solvent was evaporated under a reduced pressure, and purification was done by column chromatography on silica gel with dichloromethane as eluent (0.151 g, 33%). Mp >320 ^oC; ^1H NMR (500 MHz, $CDCl_3$) δ 8.93 (d, J = 3.57 Hz, 4H), 8.83 (d, J = 3.84 Hz, 4H), 8.21-8.23 (m, 4H), 7.99 (d, J = 8.25 Hz, 4H), 7.75-7.78 (m, 6H), 7.08 (d, J = 8.28 Hz, 4H), 4.04 (s, 4H), -2.75 (s, 2H)

S2 **S3**

Synthesis of 5,15-di(4-aminophenyl)-10,20-diphenylporphyrinatozinc(II) (1)[17]

$Zn(OAc)_2$ (0.768 g, 3.50 mmol) was dissolved in 10 mL methanol and added to 100 ml reaction flask containing **S3** (0.023 g, 0.035 mmol) in 40 mL dichloromethane. The reaction mixture was refluxed for 4 hours with continuous stirring. TLC was used to check completion of the reaction. Once the reaction was completed, the reaction mixture was poured into 50 mL water and the organic phase was extracted by adding excessive dichloromethane. After extraction, the organic layer was washed with water and brine and dried over $MgSO_4$. The solvent was evaporated under a reduced pressure, and the residue was passed through flash column chromatography on silica gel (eluent: CH_2Cl_2/CH_3OH = 100:5) to get purple powder (0.021 g, 79.3%). ^1H NMR (500 MHz, $CDCl_3$, ppm) δ 8.94 (s, 8H), 8.24 (d, 8H, J = 6.38 Hz), 7.67-7.74 (m, 12H). HR-FAB-MS: 706.1844 [M]+, calcd. for: $C_{44}H_{30}N_6Zn^+$: 706.1823

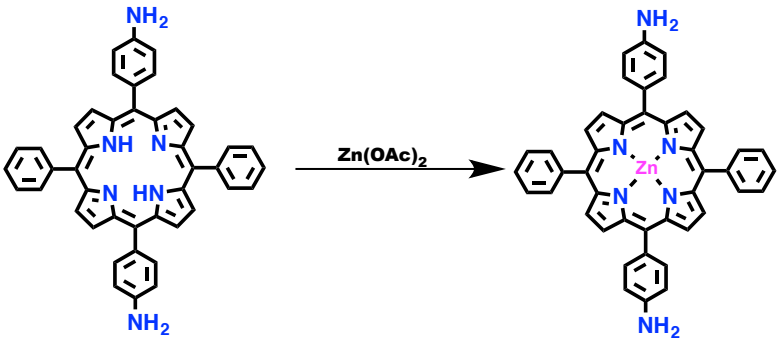

S3 **1**

2.3 Results and Discussion

2.3.1 Cyclic voltammetry

In this study, porphyrinic polymer wire **P1** was synthesized through electrooxidation method by employing three different electrodes to understand the electrochemical behavior between them. The electrodes were GC, ITO and SnO_2. Apart from that, the electropolymerization of monomer **1** to form **P1** on transparent electrodes were carried out to allow spectroscopic studies. The modification of electrode surfaces was conducted in 2.0 mM solution of **1** in 0.1 Bu_4NClO_4-CH_2Cl_2. After the polymerization was completed, the electrodes were vigorously washed with dichoromethane to ensure no monomeric porphyrin or electrolyte left on the electrode surfaces. All the modified electrodes were kept in dry condition under normal atmosphere. All the electrodes exhibit identical electrochemical behavior and exhibit good electrical conductivity as well as excellent stability.

Figure 2.3 shows a cyclic voltammogram of **1** in 0.1 M Bu_4NClO_4-CH_2Cl_2 in a repetitive redox process with scan rate as 0.2 Vs^{-1}. The increase of peak currents with the number of oxidation cycles is indicative of the formation and growth of an electroactive polymeric film on the electrode surface. A broad anodic peak with a shoulder peak was noticeable at 0.52 V vs. Ag^+/Ag, which corresponds to the oxidation of the amino group[18] and porphyrin macrocyclic rings.[19] The shoulder peak was assigned to the oxidation of the amine group due to the fact that the substituents will be oxidized before the macrocyclic ring.[20] This argument is strongly supported by the disappearance of the shoulder peaks once the electropolymerization was completed.

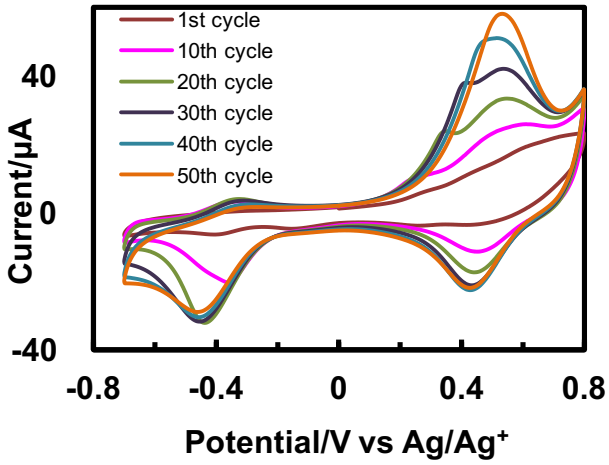

Figure 2.3: Cyclic voltammograms for **1** (2 mM) upon repetitive scans (from the 1st to 50th cycles) in 0.1 M Bu_4NClO_4–CH_2Cl_2 at GC.

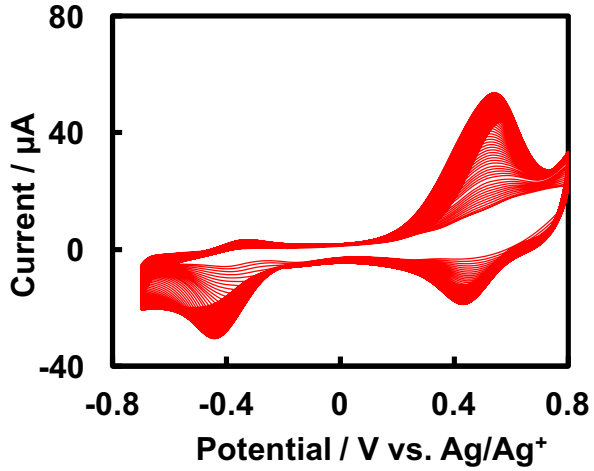

Figure 2.4: Cyclic voltammograms for **1** (2 mM) upon repetitive scans (from the 1st to 100th cycles) in 0.1 M Bu_4NClO_4–CH_2Cl_2 at GC.

When the number of scan cycles was increased up to more than 50, the polymer conductivity gradually decreased (Figure 2.4). This change might be caused by poor electron hopping between porphyrin sites when wires elongate to a certain length. Linear relationship between peak current *versus* number of scan cycles as shown in Figure 2.5 indicated the formation and growth of an electroactive film on GC surface.[21] Upon the immobilization of the polymeric film on the ITO and SnO_2, the greenish-yellow film was clearly seen to coat the electrodes surfaces. In Figure 2.6, a quasi-reversible redox wave due to [porphyrinato]zinc(II) moiety was arisen at ca. 0.52 V when the modified electrode was employed as the working electrode in blank solution (0.1 M Bu_4NClO_4-CH_2Cl_2). Besides cyclic voltammetry, differential pulse voltammetry was engaged to measure the peak maximum. In Figure 2.7, an oxidation peak was observed at ca. 0.52 V. It should be noted that the oxidation of **1** is around 0.5 V. The surface coverage of **P1** on ITO electrodes was ca. 2.7 x 10^{-9} mol cm^{-2}, estimated from the peak area of voltammograms.

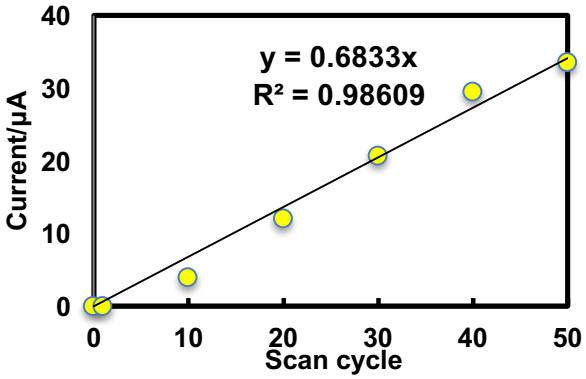

Figure 2.5: Plot of anodic peak current vs. the number of scan cycles.

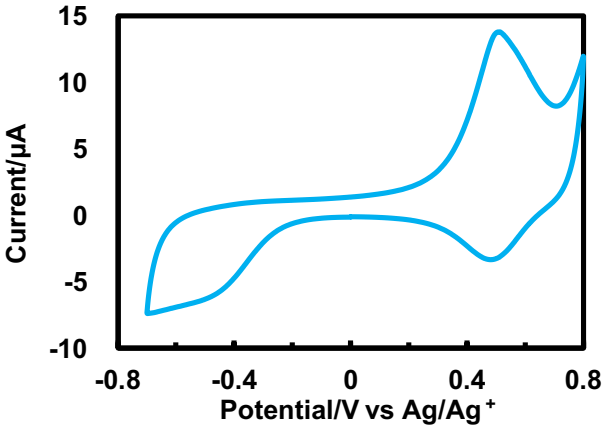

Figure 2.6: Cyclic voltammogram of **P1** on GC in 0.1 M Bu_4NClO_4–CH_2Cl_2.

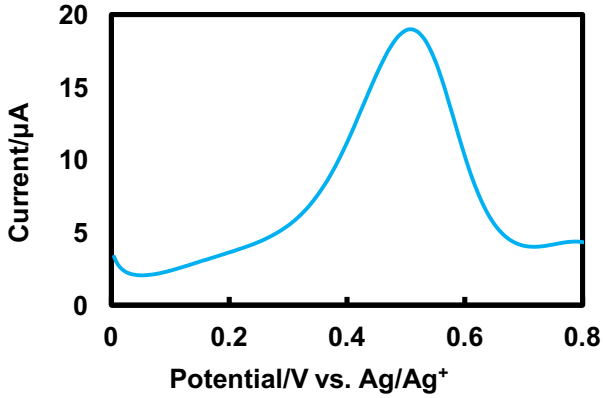

Figure 2.7: Differential pulse voltammogram for **1** in 0.1 M Bu_4NClO_4-CH_2Cl_2 at GC.

2.3.2 Comparison of electrochemical behavior between three different electrode surfaces

Three different types of electrodes were employed as the working electrodes. From the cyclic voltammograms of GC (Figure 2.10), ITO (Figure 2.11) and SnO_2 (Figure 2.12) obtained after the electropolymerization, all the electrodes exhibited similar electrochemical behavior even though the composition of three electrode materials was different. In the GC structure (Figure 2.8), there are unsaturated sp^2 carbons which allow the **P1** covalently attached to its surface. On the other hand, the differences between ITO (Figure 2.9) and SnO_2 lie only on the presence of doping atoms. Therefore, out of this differences, **P1** was successfully immobilized on all the electrodes surfaces. The identical pattern in the cyclic voltammogram between these three electrodes, indicated indeed monomer **1** can easily be immobilized on different structure of solid substrate. This versatility is really important to broaden the functionality of modified electrodes. For instance, the coated GC with electroactive film will lower the GC potential. Subsequently, it can be engaged in the electrocatalysis such as hydrogen evolution[22] and so on.

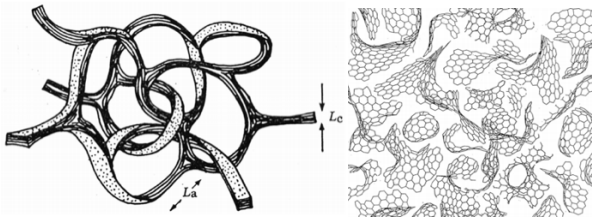

Figure 2.8: The Jenkins–Kawamura model of glassy carbon. This figure is reprint from ref. 23. Copyright 1971 Nature Publishing.

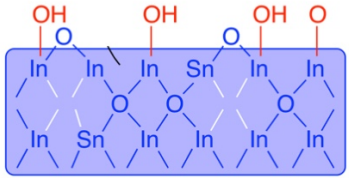

Figure 2.9: Structure of ITO. This figure is reprint from ref. 24. Copyright 2015 American Chemical Society.

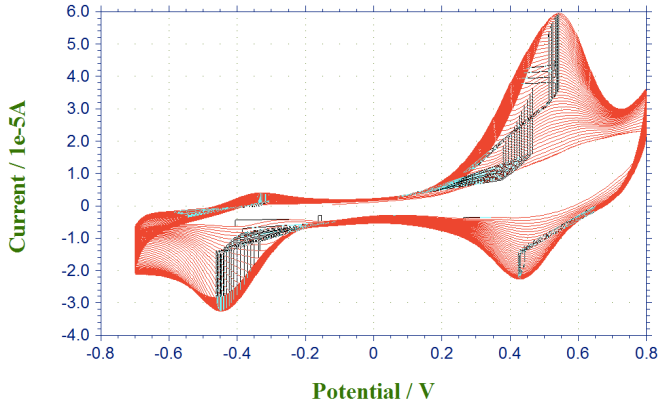

Figure 2.10: Cyclic voltammograms for **1** (2 mM) upon repetitive scans (from the1st to 50th cycles) in 0.1 M Bu_4NClO_4–CH_2Cl_2 at GC.

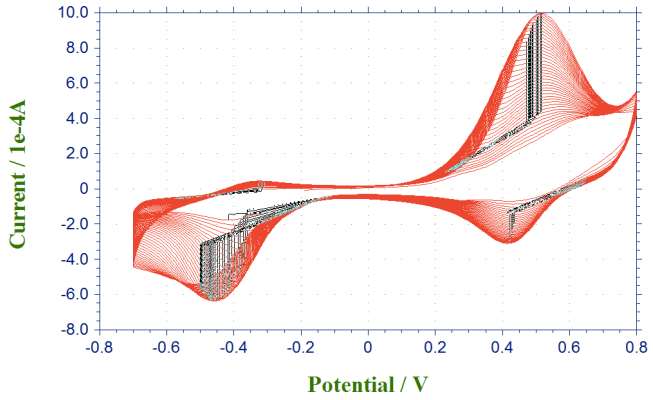

Figure 2.11: Cyclic voltammogram for **1** (2 mM) upon repetitive scans (from the 1st to 50th cycles) in 0.1 M Bu_4NClO_4–CH_2Cl_2 at ITO.

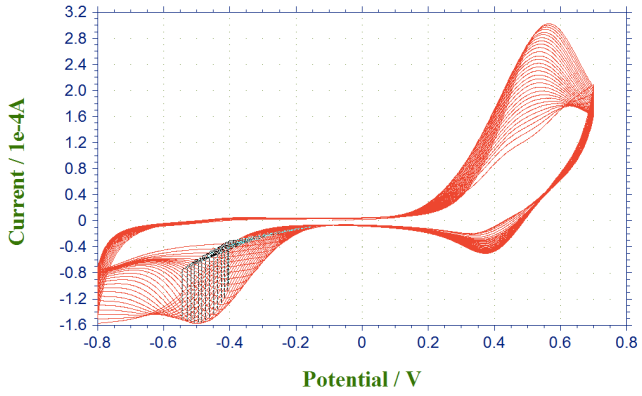

Figure 2.12: Cyclic voltammogram for **1** (2 mM) upon repetitive scans (from the 1st to 25th cycles) in 0.1 M Bu_4NClO_4–CH_2Cl_2 at SnO_2.

2.3.3 Control of film thickness

Due to their simplicity and enticing character, electrochemical polymerization has been widely used for forming numerous polymer films on the electrode surface. Subsequently, this technique also can control the film thickness. Moreover, the functionality and the uniformity of the polymeric film can be manipulated through processing parameters such as the scan rate, scan number and so forth.[25] In this study, the thickness of the polymeric film was successfully controlled by varying the number of scan cycles as well as the modifier concentration. In Figure 2.13, the film color becomes gradually darker upon increasing the number of scan cycles. This optical property changes make the polymerization easier to be monitored during experiments. The thickness of the film showed some effect on the photofunctionality of modified ITO. For instance, the thicker polymeric films showed cathodic current while the thinner film showed anodic current.

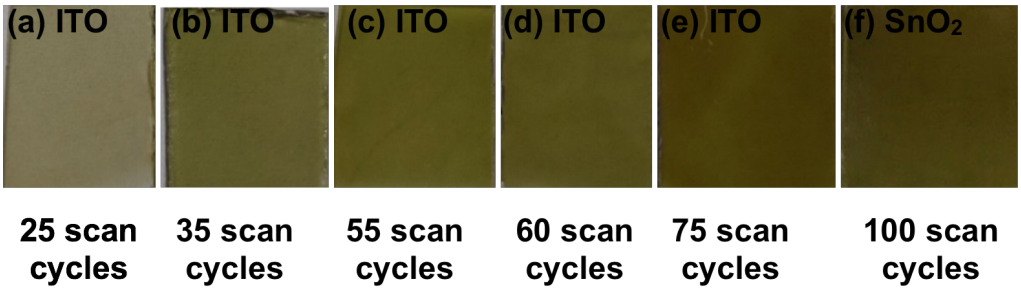

Figure 2.13: Effect of scan cycles on film color.

2.3.4 Study of surface morphology

The morphology of **P1** was investigated by AFM and SEM. In order to observe the edge of electropolymerized film, the modified electrode was scratched using utility knife, and the border of the scratched region was inspected. The surface coverage of the (porphyrininato)zinc(II) unit was estimated from the average thickness and size of **1** (Figure 2.14). Monomer **1** was estimated to have 1.8 nm height and 1.8 nm width according to DFT calculation. The 3D image of modified ITO in Figure 2.15 (a) displayed flat domain which manifested the film uniformity upon electropolymerization. From the cross-sectional profile in Figure 2.15 (b), the average thickness of **P1** varied corresponding to the difference in number of scan cycles. Table 2.1 summarizes the film thickness depending on the number of scan cycles. Film thickness will increase one fold when the scan cycles increase one fold. However, when the scan cycles went beyond the ideal number (50 scans), the film thickness deviates from this pattern. This likely happens because of slower redox reaction once the wires elongate to certain length. The amino terminal becomes harder to be oxidized and subsequently the elongation process is deteriorated.

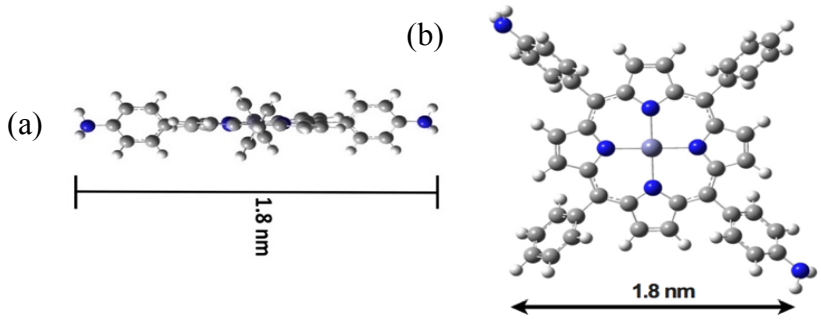

Figure 2.14: Molecular structure of monomer **1** (side view (a), and top view (b)).

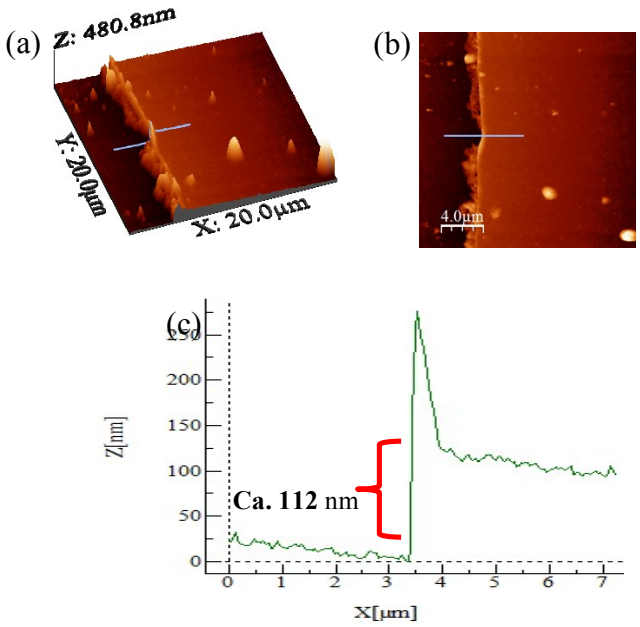

Figure 2.15: (a,b) AFM height (2D and 3D) images of an ITO electrode modified with the porphyrin polymer. (c) AFM cross-sectional profile along the blue line.

Table 2.1: Relationship between scan cycles and film thickness

The Number of scan cycles	**Film thickness (nm)**
25	60
50	112
75	120
100	200

Film images captured by optical microscope and SEM helped better understanding about the surface modification. Figure 2.16 taken by optical microscope clearly shows the physical difference between ITO and modified area. Since ITO is a transparent material, it has no color. On the other hand, the greenish-yellow domain was clearly seen in the image of modified ITO. Comparison between these two domains was clearly observed from the SEM image in Figure 2.17. Two distinguishable areas ascribed to bare ITO and polymer-attached ITO were observed. The bare ITO surface as lower part is rather smooth, whilst the area modified with **P1** as higher part displays a polymeric texture.

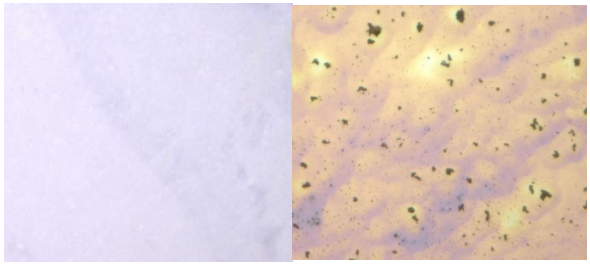

Figure 2.16: Image of bare ITO and modified ITO with **P1** taken by optical microscope.

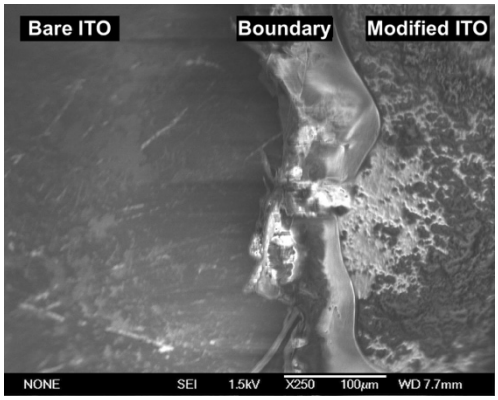

Figure 2.17: SEM image an ITO electrode modified with the porphyrin polymer, **P1**.

2.3.5 UV-vis spectroscopy

The UV-vis absorption spectra of **1** and **P1** were measured and compared to well-known zinc tetraphenylporphyrin (ZnTPP)[26] as shown in Table 2.2. Both monomer and polymer films exhibited intense light absorption in blue region which is typically observed in absorption spectra of porphyrin. In Figure 2.18, Soret band for **1** was observed at 426 nm while for **P1** it was redshifted by 4 nm. Both **1** and **P1** displayed two Q bands instead of four bands which are typical for metalloporhyrins.[27] All absorption peaks of **P1** were red-shifted compared to the absorption peaks of ZnTPP due to the longer conjugated carbon chain in **P1**. The similarity between Soret band and Q bands of **P1** to monomer **1**, indicates that the porphyrin skeleton was maintained upon electropolymerization. Therefore, this immobilization method is found to be decent to immobilized porphyrin monomer with anilino substituents due to the fact that the stability of porphyrin macrocyclic rings could be maintained during the electropolymerization. The relationship between scan cycles and light absorption of **P1** was shown in Figure 2.19. The film formed after 100 cycles has the maximum light absorption while the thinnest film fabricated upon 5 cycles does the smallest absorbance. Indeed, these absorption spectra verified the correlation between scan cycles and film thickness.

Table 2.2: Visible absorption maxima of ZnTPP, **1** and **P1**.

	ZnTPP	**1**	**P1**
Soret Band (nm)	422	426	430
Q bands (nm)	512 548 589	- 556 598	- 562 610

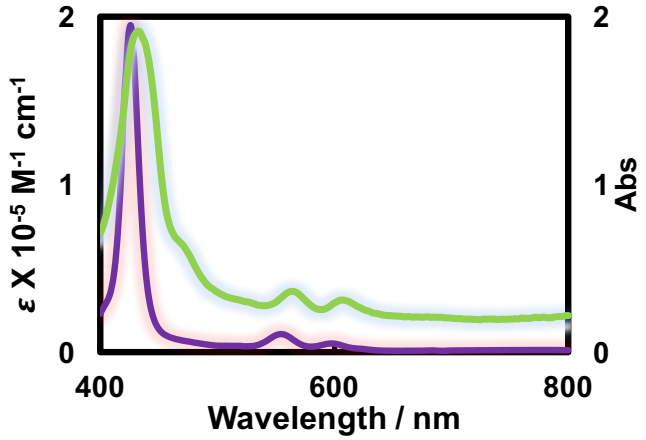

Figure 2.18: Absorption spectra of **1** (purple line) in dichloromethane and **P1** (green line) on ITO.

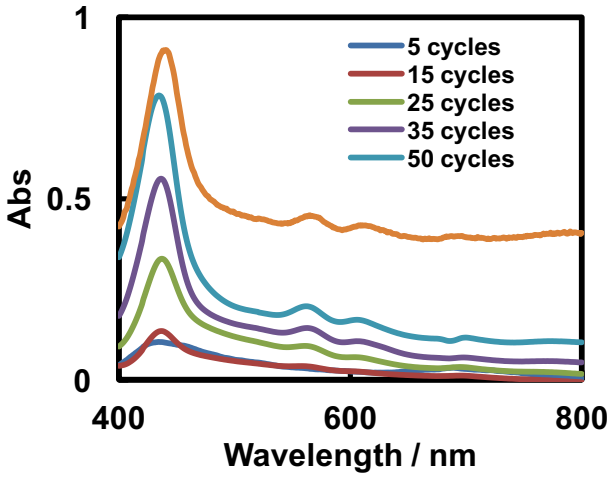

Figure 2.19: The relationship between the absorption of **P1** and the number of scan cycles for electropolymerization.

2.3.6 Fluorescence spectroscopy

Upon light excitation, **1** exhibit fluorescence emission at certain wavelengths. The emission spectra of **1** (Figure 2.20) were measured for excitation wavelength of 427 nm, 552 nm and 593 nm in toluene. Excitation to the S_2 (Soret Band) and S_1 (Q bands) in **1** results in fluorescence. The fluorescence of Soret band is caused by transition from the second excited singlet state S_2 to the ground state, S_0. On the other hand, the fluorescence of Q bands is transition from the lowest excited singlet state S_1 to the ground state, S_0. The fluorescence bands of **1** were at 608 nm and 650 nm which are red-shifted compared to the fluorescence bands of ZnTPP in dichloromethane appearing at 592 nm and 642 nm,[28] respectively.

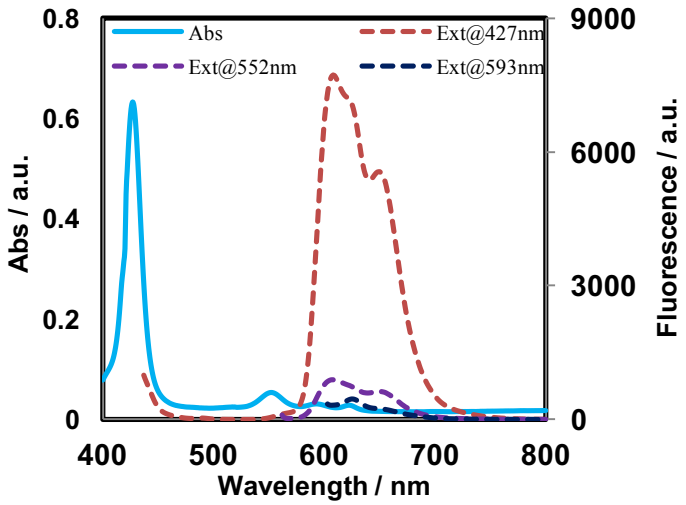

Figure 2.20: Absorption spectra of **1** (blue line) in toluene and fluorescence emission of **1** in toluene.

2.3.7 Study of azobenzene linkage by Raman spectroscopy

The presence of azobenzene linkage in **P1** was investigated by means of Raman spectroscopy and compared with the well-known *trans*-azobenzene spectrum. Raman scattering is known to exhibit strong intensity for modes with C-N and N=N vibrations except for C-H displacements. In this research, Raman spectra of **1** and **P1** (Figure 2.21) were recorded with JASCO NRS-5100 using the probe light at 532 nm. In the case of trans-N-benzylideneanilene,[29] there are five distinguished bands in the range of 1640-1400 cm^{-1}. These bonds can be assigned to four bands of ring stretching vibrations known as Wilson modes 8a, 8b, 19a,19b[30] and the bond above 1600 cm^{-1} is assigned to double bond either C=C or C=N. Therefore, peaks **1** and **2** were assigned to ring stretching. While, peak **4** was ascribed to ring vibration. A doublet band due to ring and ring substituents stretching is usually observed in this wavenumber range.

In the Raman spectrum of *trans*-azobenzene, bands above 1600 cm^{-1} are absent but two bands are present between 1500 and 1450 cm^{-1}, which are assignable to 19a and 19b modes. In the past, N=N stretching were suggested to be at 1439[31] and 1472 cm^{-1} [32] but more recent studies revealed that azo stretching[33,34,35] mode is at 1440 cm^{-1} instead of at higher wavelength as previously reported. On the other hand, another Raman active azo band at 1143 cm^{-1} corresponding to N=N-Ph symmetric bend was also reported.[35] In the Raman spectrum of **P1**, a characteristic band was discovered at 1446 cm^{-1}, whereas it was unnoticeable in **1**. This strong peak was assigned to N=N stretching vibration of the azo group.[36] This peak also appeared in the theoretical Raman spectrum of **P1** (Figure 2.22) obtained by DFT calculation. The similarities between the theoretical and experimental Raman spectra support the existence of –N=N- in **P1** structure. The shifting in frequency of N=N stretching is probably affected by the mixing signal between ring and bridging group vibrations. Thus, this upshift indicates that there is a strong coupling between N=N stretching and ring stretching vibrations.

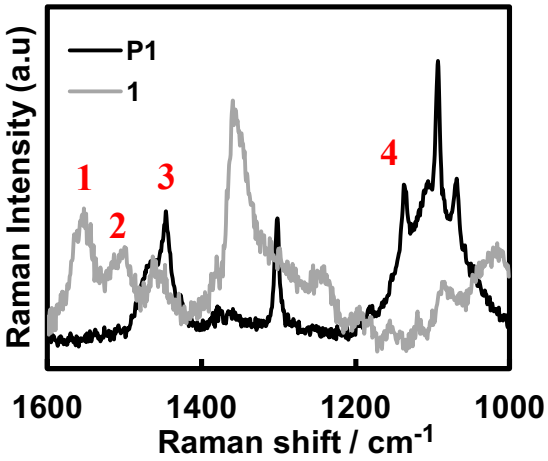

Figure 2.21: Raman spectra of **1** and **P1**.

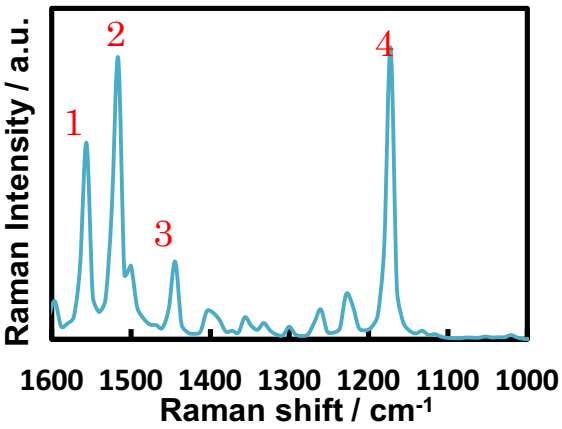

Figure 2.22: Theoretical Raman spectrum of **P1** obtained by DFT calculation. (cf. N=N stretch in azobenzene spectrum[36]).

2.3.8 X-ray photoelectron spectroscopy (XPS)

P1 was subjected to X-ray photoelectron spectroscopy (XPS) in order to analyze their constitutive elements. Figure 2.23 (a) shows the survey scan for **P1** on ITO with ca. 112 nm thickness, while Table 2.3 summarizes the binding energy for related elements. As shown in Figure 2.23 (b), two different nitrogen atoms are present in **P1** structure. In Figure 2.24, the nitrogen peak fitting was done to understand the nitrogen atoms chemical environment in **P1** structure. Two nitrogen peaks at 397.5 eV and 399.2 eV, whose peak ratio close to 2:1 were identified in the (porphyrininato)zinc(II) polymeric film. At 397.5 eV, the N=N nitrogen atoms[37] were directly attached to the conjugated system which may influence the binding energy value. On the other hand, the peak at 399.2 eV could be assigned to iminic nitrogen atoms at porphyrin ring which coordinated to zinc ion[38]. The zinc $2p_{2/3}$ (Figure 2.24) was observed at 1021.02 eV. The abundance ratio between nitrogen 1s and zinc $2p_{2/3}$ was calculated from the peak areas corrected using the photoionization cross-section, which was consistent with the expected values of N:Zn = 6:1 (found 1.5:6.5). This ratio indicates the formation of azobenzene linkage in **P1**.

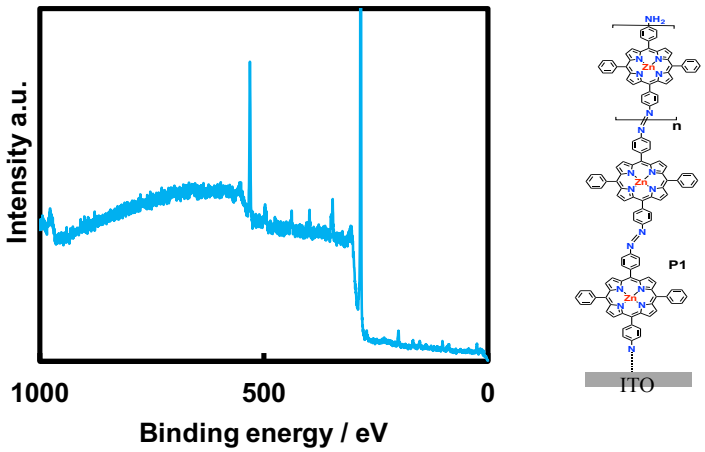

Figure 2.23: (a) XPS spectra of survey scan of peak assignment for **P1** on ITO (ca. thickness 112 nm). (b) Expected chemical structure with different N atoms in **P1**.

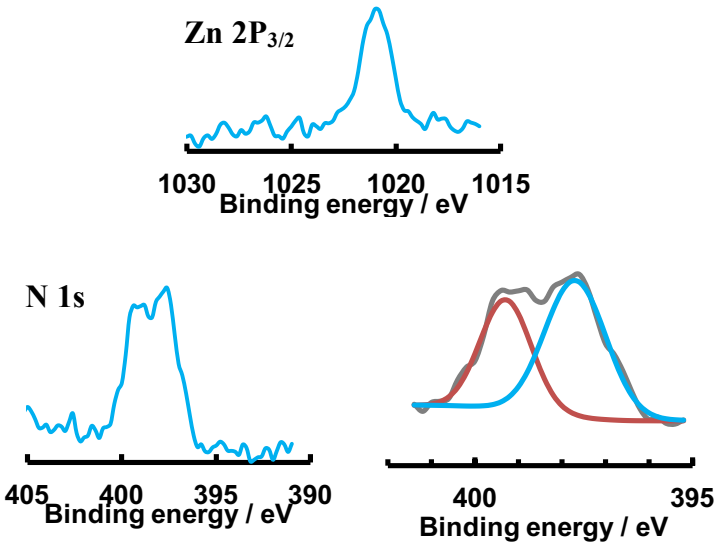

Figure 2.24: Narrow-scan XPS for **P1**, (a) focusing on the Zn $2p_{3/2}$ region, and (b) focusing on the N 1s region. (c) Deconvolution spectra of N 1s.

Table 2.3: Binding energies (eV) of elements in **P1**

Signal	**Binding energy / eV**
N 1s	399.2 , 398.0
Zn $2p_{3/2}$	1021.02
C 1s	283.9
O 1s	287.4, 531.2

2.4 Polymerization Mechanism

In this study, various characterization techniques were employed to study the **P1** polymeric structure. From these studies, a plausible polymerization mechanism as shown in Figure 2.26 was proposed. The attachment of **P1** on electrode surfaces was disclosed through cyclic voltammetry. The electrooxidation of **P1** initiates the polymerization, which is started by the formation of reactive anilino radicals.[39] Subsequently, one of the anilino radicals was tethered on the electrode surface which C=C bonds serving as electrophiles and the amine group acting as nucleophiles. Figure 2.25 shows the formation of C-N bonds between GC and the amine [40,41,42,43,44]. The nucleophilic attack of anilino radical at electrophilic C=C sites on GC surface leads to the formation of covalent bond. In the case of ITO and SnO_2, although the electrochemical and XPS measurements proved the immobilization of monomer **1** on ITO surface through the electrochemical manner, the nature of the linkages between the anilino radical and ITO surface including the exact mechanism of oxidative attachment remain unclear. However, a plausible mechanism had been reported between carbon and ITO surfaces. The modification expects to occur through bond formation between a carbon radical that bind to the surface hydroxyl groups or strongly physisorbed onto the ITO surface.[24] The growth of **P1** is enabled by the coupling between two anilino radical species which one is tethered on the electrode surface while the other one is in the solution phase. The coupling between two anilino radical forms hydrazine linkage, which undergoes electrochemical oxidation to azobenzene linkage. The presence of the azobenzene linkage in **P1** structure was identified by Raman spectroscopy and the preservation of porphyrinic moiety upon electrooxidation was indicated by UV/vis spectroscopy.

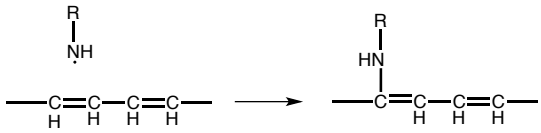

Figure 2.25: The formation of CN bond between GC and anilino radical.

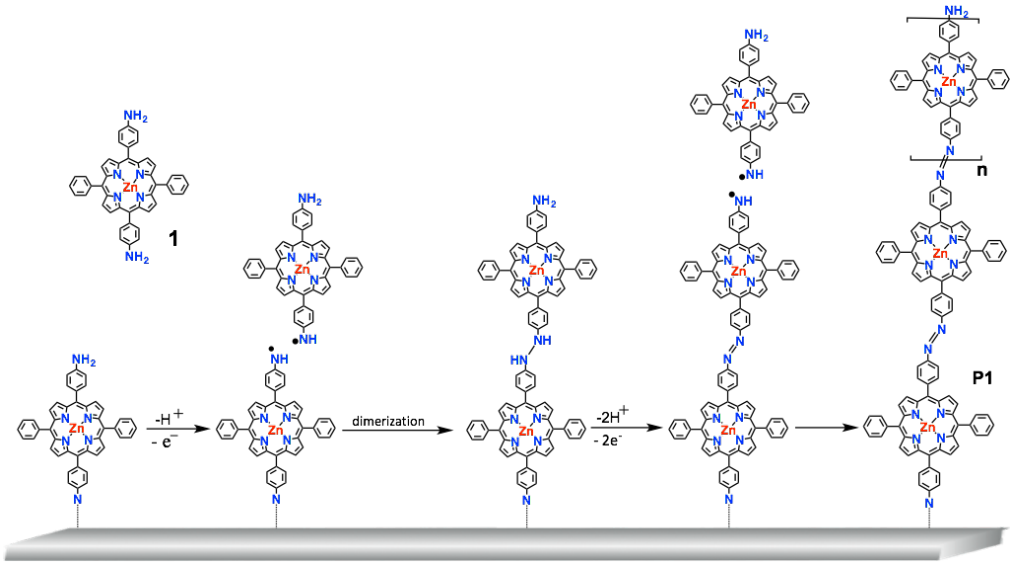

Figure 2.26: Proposed mechanism of the oxidative electropolymerization of **1** to form **P1**.

2.5. Photofunctionality

2.5.1 Photoelectric conversion

The modified ITO was expected to show photofuctionality. Therefore, a three-electrode electrochemical cell was employed to measure the photoelectric conversion ability. The insignificant dark current was observed when the potential of the photoanode fixed close to the open circuit potential (−0.22 V vs. Ag/Ag^{+}). A stable anodic photocurrent appeared immediately upon irradiation of ITO electrode with λ = 440 nm light as shown in Figure 2.27. This demonstrates that photocurrent flows from the electrolyte to ITO electrode via **P1** polymeric films. The photocurrent fell down instantly when the illumination was cut off. The maximum quantum yield for the photoelectric conversion was around 0.04%. One possible reason behind the low quantum yields is some part of modified ITO which might be suffered from film defect. Eventually, size of electrode active area is approximated from size of fluorocarbon O-ring. Therefore, if the defect area was included in electrode active area during photocurrent generation measurement, it might affect the amount of photon being absorbed and subsequently cause low quantum yield. The calculation for quantum yield of photocurrent generation was made according to a previous literature.

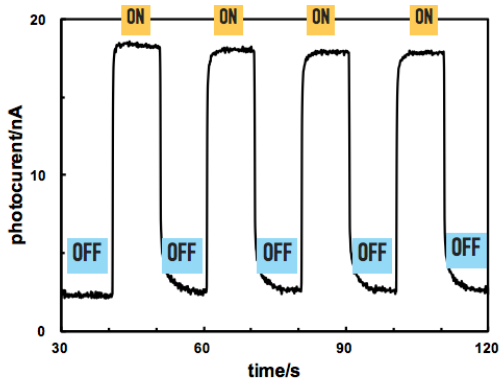

Figure 2.27: Generated anodic photocurrent upon light irradiation at 440 nm.

2.5.2 Wavelength dependency

The features of photocurrent action spectra roughly resemble their respective absorption spectra. The agreement of the photoaction spectrum normalized to photon numbers with absorption spectrum of modified ITO with **P1** from 400–500 nm (Figure 2.27) demonstrates clearly that the porphyrin is the photoactive species. The maximum photocurrent value was observed at porphyrin Soret band, which strongly indicates that porphyrin moiety was responsible in the photocurrent generation. The action spectrum showed a deviation from absorption spectrum, indicated the maximum absorption band's wavelength is not consistent with the wavelength of the highest photocurrent.[45] This blue shift in the photocurrent action spectrum might be caused by the solvent effects in UV-vis absorption measurement. Besides that, introduction of bias potential during measurement or light irradiation might significantly affect the orientation of the wires which prone to tilted or vice versa. This hypothesis was deduced from the fact that the azobenzene-bridged porphyrin can change their conformations under external stimulation.[46]

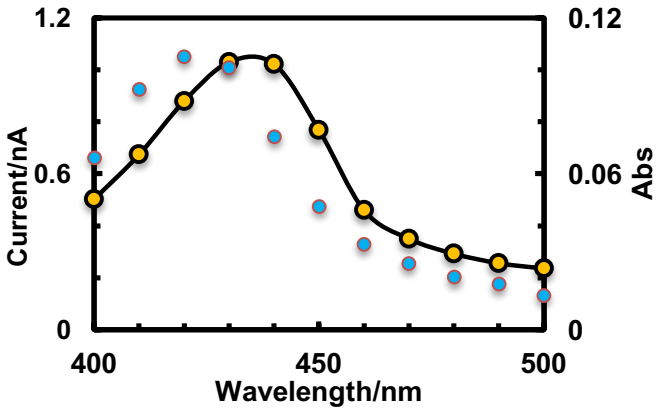

Figure 2.27: Action spectrum for the photocurrent generation (blue dots) and the absorption spectrum of **P1** on an ITO substrate (black solid line with yellow dots).

2.5.3 Proposed mechanism for photoelectric conversion

In order to understand in depth, the electron transfer reactions, photocurrent generation was observed by applying bias voltage on working electrode (I−V curve) to change the relative HOMO and LUMO position against ITO Fermi level. The HOMO value of **P1** was estimated from the oxidation potential measured by cyclic voltammetry. Whilst, the LUMO level of **P1** was calculated from absorption peak wavelength of 562 nm, which is converted to energy by employing equation 2.1.

$$E=hc/\lambda \qquad \text{Equation 2.1}$$

Figure 2.28 shows the plausible energy diagram of an ITO electrode, **P1** and TEOA. In this electron transfer scheme, when the light is irradiated to **P1**-modified ITO, the electron in an occupied molecular orbital is excited to an unoccupied molecular orbital. Subsequently, an electron is transferred from **P1** to ITO Fermi level. Hence, TEOA as sacrificial reagent will donate an electron to hole in **P1**.

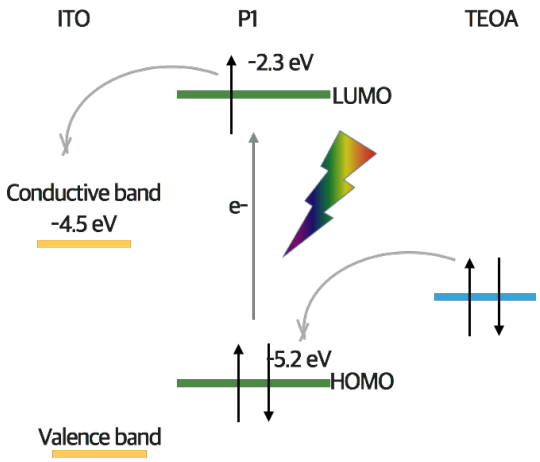

Figure 2.28: Schematic diagram of the plausible energy diagram of a modified ITO electrode, **P1** and TEOA.

2.6 Conclusion

Characterization of **P1** were conducted by various methods in order to get better understanding. The morphology of **P1** was studied by employing AFM and SEM, while XPS, Raman and UV-vis spectroscopy were utilized to investigate the composition of the polymeric film of **P1**. Microscopic measurement disclosed that **P1** had polymeric structure and spectroscopic study suggested the presence of azobenzene linkage in **P1**. These results indicate that the one-dimensional molecular wire was successfully generated through the electrooxidation of anilino substituents in the porphyrinatozinc(II) complex structure. Meanwhile, **P1** showed the photoelectric conversion ability with the maximum internal quantum yield of 0.04%.

2.7 References

1. Cirera, B., Gimenez-Agullo, N., Bjork, J., Martinez-Pena, F., Martin-Jimenez, A., Rodriguez-Fernandez, J., Pizarro, A. M., Otero, R., Gallego, J. M., Ballester, P., Galan-Mascaros, J. R. and Ecija, D. Thermal selectivity of intermolecular versus intramolecular reactions on surfaces. *Nat. Commun.* **7,** 11002 (2016).
2. Alemayehu, A. B., Day, N. U., Mani, T., Rudine, A. B., Thomas, K. E., Gederaas, O. A., Vinogradoy, S. A., Wamser, C. C. and Ghosh, A. Gold tris(carboxyphenyl) corroles as multifunctional materials: Room temperature near-IR phosphorescence and applications to photodynamic therapy and dye-sensitized solar cells. *ACS Appl. Mater. Interfaces*. **8**, 18935-18942 (2016).
3. Zhang, L., Wang, K., Qian, X., Liu, H. and Shi, Z. Porous conjugated polymer nanotip arrays for highly stable field emitter. *ACS Appl. Mater. Interfaces* **5,** 2761–2766 (2013).
4. Huang, S.-C. and Lin, C.-Y. Reductive electropolymerization of N-methyl-3-pyridylethynyl-porphyrins. *Chem. Commun.* **51,** 519–521 (2015).
5. Gross, A. J., Bucher, C., Coche-Guerente, L., Labbe, P., Downard, A. J. and Moutet, J-C. Nickel (II) tetraphenylporphyrin modified surfaces via electrografting of an aryldiazonium salt. *Electrochem. commun.* **13,** 1236–1239 (2011).
6. Hebié, S., Dimé, A. K. D., Devillers, C. H. and Lucas, D. Electrochemistry as an attractive and effective tool for the synthesis and immobilization of porphyrins on an electrode surface. *Chem. - A Eur. J.* **21,** 8281–8289 (2015).
7. Chiu, K-Y, Chung, Y-C. and Su, O. Y. Effects of azo bridge and substituents on the electrochemical and spectral properties of bis(triarylamine)s. J. Chinese Chemical Society, **53**,1413–1418 (2006).
8. Yao, J., You, J., Lei, Y. and Dong, L. Main-chain azo polyaramides with high thermal stability and liquid crystal properties. *J. Polym. Res*. **16**, 455-460 (2009).
9. Peng, S., Guo, Q., Hartley, P. G. and Hughes, T. C. Azobenzene moiety variation directing self- assembly and photoresponsive behavior of azo- surfactants. *J. Mater. Chem. C*. **2**, 8303-8312 (2014).
10. Zhou, X., Ren, H., Chen, H. and Wang, M. Synthesis and photoconductivity study of azo. *J. Appl. Polym. Sci.* **73,** 1913–1920 (1999).

11. Kumar, G. S. and Neckers, D. C. Photochemistry of azobenzene-containing polymers. *Chem. Rev.* **89,** 1915–1925 (1989).
12. Delaire, J. A. and Nakatani, K. Linear and nonlinear optical properties of photochromic molecules and materials. *Chem. Rev.* **100**, 1817-1845 (2000).
13. Yamada, H., Imahori, H., Fukuzumi, S., Nishimura, Y. and Yamazaki, I. Remarkable enhancement of photocurrent generation by ITO electrodes modified with a self-assembled monolayer of porphyrin. *Chem. Commun.***19**, 1921–1922 (2000).
14. Lin, T., Shang, X. S., Adisoejoso, J., Liu, P. N. and Lin, N. Steering on-surface polymerization with metal-directed template. *J. Am. Chem. Soc.* **17,** 1–9 (2013).
15. Boccalon, M., Iengo, E. and Tecilla, P. New meso-substituted trans-A_2B_2 di(4-pyridyl)porphyrins as building blocks for metal-mediated self-assembling of 4 + 4 Re(I)–porphyrin metallacycles. *Org. Biomol. Chem.* **11,** 4056–4067 (2013).
16. Chauhan, S. M. S. and Giri, N. G. Rosette formation by hydrogen bonding of 5,5-dialkylbarbituric acids with 2-amino-4,6-bi[5-(4′-aminophenyl)porphyrinatozinc]-1,3,5-triazines in solution. *Supramol. Chem.* **20,** 743–752 (2008).
17. He, C., He, Q., Deng, C., Shi, L., Zhu, D., Fu, Y., Cao, H. and Chemg, J. Turn on fluorescence sensing of vapor phase electron donating amines via tetraphenylporphyrin or metallophenylporphrin doped polyfluorene. *Chem. Commun.*. **46,** 7536–7538 (2010).
18. Rodney L. Hand, R. F. N. Anodic oxidation pathways of N-alkylanilines. *J. Am. Chem. Soc.* 850–860 (1974)
19. Kadish, K. M. and Rhodes, R. K. Reactions of Metalloporphyrin. *Inorg. Chem.* **20,** 2961–2966 (1981).
20. Bettelheim. A, White. B. A, Raybuck. S. A and Murray R. Electrochemical polymerization of amino-, pyrrole-, and hydroxy-substituted tetraphenylporphyrins. *Inorg. Chem.* **26,** 1009–1017 (1987).
21. Nishihara, H., Noguchi, M. and Aramaki, K. Synthesis of ferrocene and cobaltocene electrode films by electropolymerization and their spectral and electrochemical properties. *Inorg. Chem* **26,** 2862–2867 (1987).

22. Canales, C., Felipe, V-C., Thomas E. M., Ramirez, G. Enhanced electrocatalytic hydrogen evolution reaction: Supramolecular assemblies of metalloporphyrins on glassy carbon electrodes. *Appl. Catal. B Environ.* **188,** 169–176 (2016).
23. Jenkins, G. M. and Kawamura, K. Structure of glassy carbon. *Nature* **231,** 175–176 (1971).
24. Charlton, M. R., Suhr, K. J., Holliday, B. J. and Stevenson, K. J. Electrochemical modification of indium tin oxide using di(4-nitrophenyl) iodonium tetrafluoroborate. *Langmuir* **31,** 695–702 (2015).
25. Han, S., Briseno, A. L., Shi, X., Mah, D. A. and Zhou, F. Polyelectrolyte-coated nanosphere lithographic patterning of surfaces: Fabrication and characterization of electropolymerized thin polyaniline honeycomb films. *J. Phys. Chem. B* **106,** 6465–6472 (2002).
26. Barnett, G. H., Hudson, M. F. and Smith, K. M. Concerning meso-tetraphenylporphyrin purification. *J. Chem. Soc. Perkin Trans. 1*,1401 (1975).
27. Gouterman, M. Spectra of Porphyrins. *J. Mol. Spectrosc.* **6,** 138–163 (1961).
28. Huang, C.-Y. and Su, Y. O. Spectral and redox properties of zinc porphyrin core dendrimers with triarylamines as dendron. *Dalton Trans.* **39,** 8306–8312 (2010).
29. Meic, Z. and Baranovic, G. Vibrational spectra of trans-N-benzylideneaniline and its isotopomers. *Pure Appl. Chem.* **61,** (1989).
30. Wilson, E. B. The normal modes and frequencies of vibration of the regular plane hexagon model of the benzene molecule. *Phys. Rev.* **45,** 706–714 (1934).
31. Kellerer, B., Brandmul. J and Hacker, H. Structure of azobenzene and tolane in solution - Raman spectra of azobenzene, azobenzene-D10, para-,para'-azobenzene-D2, azobenzene-n-15=n-15 and tolane. *Indian J. Pure Appl. Phys.* **9,** 903(1971).
32. Gruger, A., Dizabo, P. and Lecalve, N. Vibration-spectra of trans azobenzene and isotopic derivatives. *J. Chim. Phys. PCB* **69,** 291 (1972).
33. Meić, Z., Baranovic, G., Smreccki, V., Novak, P., Keresztury, G. and Holly, S. Vibrational coupling in trans-azobenzene and its isotopomers. *J. Mol. Struct.* **408-409,** 399–403 (1997).
34. Koide, S., Udagawa, Y., Mikami, N., Kaya, K. and Ito, M. The resonance Raman

effect. *Bul. Chem. Soc. Japan* **45,** 3542–3543 (1972).

35. Armstrong, D. R., Clarkson, J. and Smith, W. E. Vibrational analysis of trans-Azobenzene. *J. Phys. Chem* **99,** 17825–17831 (1995).
36. Liu, Y. C. and McCreery, R. L. Raman spectroscopic determination of the structure and orientation of organic monolayers chemisorbed on carbon electrode surfaces. *Anal. Chem.* **69,** 2091–7 (1997).
37. Chen, S., Bao, L., Ou, E., Peng, C., Wang, W. and Xu, W. A cationic azobenzene-surfactant-modified graphene hybrid: Unique photoresponse and electrochemical behavior. *Nanoscale* **7,** 19673–19686 (2015).
38. Kretschmann, A., Walz, M-M, Flechtner, K., Steinruck, H-P. and Gottfried, J. M. Tetraphenylporphyrin picks up zinc atoms from a silver surface. *Chem. Commun.* **128,** 568–570 (2007).
39. Deinhammer, R. S., Ho, M., Anderegg, J. W. and Porter, M. D. Electrochemical oxidation of amine-containing compounds: A route to the surface modification of glassy carbon electrodes. *Langmuir* **10,** 1306–1313 (1994).
40. Barbier, B. Electrochemical bonding of amines to carbon fiber surfaces toward improved carbon-epoxy composites. *J. Electrochem. Soc.* **137,** 1757 (1990).
41. González-Fuentes, M. A., Daáz-Sánchez, B. R., Vela, A. and González, F. J. Radical grafting of carbon surfaces by oxidation of 5-nitroindole derived anions. *J. Electroanal. Chem.* **670,** 30–35 (2012).
42. Bélanger, D. and Pinson, J. Electrografting: A powerful method for surface modification. *Chem. Soc. Rev.* **40,** 3995–4048 (2011).
43. Yang, G., Liu, B. and Dong, S. Covalent modification of glassy carbon electrode during electrochemical oxidation process of 4-aminobenzylphosphonic acid in aqueous solution. *J. Electroanal. Chem.* **585,** 301–305 (2005).
44. Yang, G., Shen, Y., Wang, M., Chen, H., Liu, B. and Dong, S. Copper hexacyanoferrate multilayer films on glassy carbon electrode modified with 4-aminobenzoic acid in aqueous solution. *Talanta* **68,** 741–747 (2006).
45. Schlettwein, D., Kaneko, M., Yamada, A., Woehrle, D. and Jaeger, N. I. Light-induced dioxygen reduction at thin film electrodes of various porphyrins. *J. Phys. Chem* **95,** 1748–1755 (1991).

46. Huang, W., Lee, S-K., Sung, Y. M., Peng, F., Yin, B., Ma, M., Chen, B., Liu, S., Kirk, S. R., Kim, D. and Song, J. Azobenzene-bridged porphyrin nanorings: Syntheses, structures, and photophysical properties. *Chem. - A Eur. J.* **21,** 15328–15338 (2015).

CHAPTER 3　（要約）

Bis(dipyrrinato)zinc(II) Linked Porphyrin Wires

CHAPTER 4
CONCLUDING REMARKS

In Chapter 1, the porphyrin and its derivatives were briefly introduced. As mentioned before, porphyrins are among the most versatile compounds with interesting features which have potentials to be utilized in many areas. Apart from that, porphyrin also can be polymerized on many solid supports such as glassy carbon, ITO, SnO_2 and so forth. Self-assembly is one of the pathways to fabricate highly ordered porphyrin polymers. However, this modification is primarily based on monolayer systems with simple structures. Therefore, stepwise coordination becomes more favorable for more complex structures. In the case of fabricating multilayer structures, electrochemical polymerization offers several advantages that are significantly attractive and worth to be explore extensively. In this research, the polymerization of porphyrinic monomers bearing anilino substituents was engaged to fabricate azobenzene-linked porphyrin wires on GC, ITO and SnO_2. Besides electropolymerization, metal complexation reaction was also successfully explored to synthesize a porphyrinic wires which are linked by bis(dipyrrin)zinc(II) moiety.

Comprehensive discussion regarding azobenzene-linked porphyrinic wires formed by electrochemical polymerization has been compiled in Chapter 2. Electrochemical polymerization is chosen due to simplicity in polymerization process. In this chapter, synthesis of monomer **1,** its electrochemical polymerization mechanism, and characterization of the formed polymer, **P1** were thoroughly explained. Various characterization techniques were employed and the results verified the present of azobenzene linkage in **P1** structure. The effect of scan cycles was studied by measuring several different electrodes with different thickness. The AFM results disclosed few scan cycles resulting to thin film while repetitive scan cycles grow thicker film. Besides characterization, the functionality of **P1** was explored through photoelectric conversion measurement. **P1** was successfully employed as photoanode and anodic photocurrent was observed upon light irradiation with 0.04% quantum efficiency. This finding marks the potential of **P1** to be utilized in fabrication of optoelectronic devices in future.

Besides electrochemical polymerization, other techniques such as metal complexation reaction also has capability to fabricate porphyrinic wires by introducing substituents bearing coordination sites to porphyrin macrocycles at meso positions. In the research in Chapter 3, dipyrrin moiety was chosen due to its great features such as

remarkable optical and electronic properties. Complexation between free base dipyrrin moiety with zinc(II) cation in a simple manner opens the possibilities to engage **W2** in materials science. Therefore, functionality of **W2** has been studied and the result turns out that **W2** has ability to be utilized as photoanode in photocurrent generation. Owing to the hybridization between porphyrin and dipyrrin compound, **W2** was found to exhibit better quantum efficiency (0.19%) and much wider light absorption range. Let alone porphyrin moiety, the intense light absorption will be limited around 400-450 nm (Soret band) but by introducing the dipyrrin moiety, the absorption wavelength range become much broader exceeding 500 nm.

In summary, synthesis of one-dimensional porphyrinic wires by electropolymerization and metal complexation reaction were achieved. The photofunctionality of both wires were adequately explored. Both wires were found to exhibit photocurrent generation abilities. These studies open the possibilities for both wires to be utilized in the fabrication of electronic and optoelectronics applications.

A**cknowledgement**

First and foremost, I would like to express my appreciations to Prof. Hiroshi Nishihara, my supervisor, for his kindness, advice, care, and guide that were offered to me to enrich my scientific career. Secondly, I would like to thank the Japan Government for the funding of my study throughout these three years. I also would like to thank Associate Professor Dr. Yoshinori Yamanoi, Assistant Professor Dr. Ryota Sakamoto, Assistant Professor Dr. Tetsuro Kusamoto, Project Assistant Professor Dr. Mariko Miyachi, Project Assistant Professor Dr. Hiroaki Maeda and Project Assistant Professor Dr. Kuo-Hui Wu for helping me in my research by giving continuous help and assistance. This work would not have been possible without continuous help, meaningful discussions and great working atmospheres. I am really thankful to be giving the opportunity to work with kind-hearted and knowledgeable people in Nishihara group especially former and present Room 2604 members: Mr. Kazuyuki Aonuma, Mr. Tatsuhiro Nagayama, Mr. Ryojun Toyoda, Mr. Ryota Matsuoka, Mr. Mizuho Tsuchiya, Mr. Toshiki Iwashima, Mr. Ukyo Nakajima, Mr. Xinsen Sun, Ms. Eunice Phua, Ms. Risa Aoki and Ms. Borines Ma. Leah Maramara. I also would like to show special thanks to Dr. Yusuke Takara, Dr Kenji Takada and Mr. Toshiki Yagi for their kindness and Mr. Pal Tigmansu who is in the same batch as me. Last but not least, I would like to thank all members of Inorganic Chemistry laboratory including Ms. Tomomi Funabiki and Ms. Yumiko Hosoya for helping me unconditionally throughout these years. I do appreciate and enjoyed the moments I spent here.

To my family and friends, thank you for your continuous support and unconditional love.

I feel blessed by the chance to meet and learn from different people and that were eye-opening experiences.

Alhamdulillah

Suzaliza Mustafar, July 2016.

Publication List

[Publication related to the thesis**]**

1. "Electrochemical fabrication of one-dimensional porphyrinic wires on electrodes" Suzaliza Mustafar, Kuo-Hui Wu, Ryojun Toyoda, Kenji Takada, Hiroaki Maeda, Mariko Miyachi, Ryota Sakamoto and Hiroshi Nishihara, *Inorg. Chem. Front.* **3**, 370-375 (2015).

[Publication not related to the thesis**]**

1. "Meso-N-arylamino- and N,N-diarylaminoporphyrinoids: Syntheses, properties and applications" Ryota Sakamoto, Suzaliza Mustafar and Hiroshi Nishihara, *J. Porphyr. Phthalocya*., **19**, 1–11(2015)**.**
2. "A highly selective Copper(II) Electrode based on PVC membrane of 2-Acetylpyridine-(1R)-(-)-Fenchone Azine ligand" Illyas Md Isa, Mohamad Idris Saidin, Mustaffa Ahmad, Suzaliza Mustafar and Sazelli A Ghani, *Int. J. Electrochem. Sci*., 9526-9536 (2012).
3. "Cobalt (II) selective membrane electrode based on Palladium(II) dichloroacetylthiophene azine" Illyas Md. Isa, Suzaliza Mustafar, Mustaffa Ahmad, Norhayati Hashim and Sazelli A. Ghani , *Talanta*, **87**, 230-243 (2011).